Apoptotic signaling clears engineered *Salmonella* in an organ-specific manner

Taylor J. Abele[1,2,3], Zachary P. Billman[1,2,3,4], Lupeng Li[1,2,3], Carissa K. Harvest[1,2,3,4], Alexia K. Bryan[1,5], Gabrielle R Magalski[4], Joseph P Lopez[4], Heather N. Larson[1,2,3], Xiao-Ming Yin[6], and Edward A. Miao[1,2,3,*]

[1] Department of Integrative Immunobiology, Duke University School of Medicine, Durham, NC, USA 27710

[2] Department of Molecular Genetics and Microbiology, Duke University School of Medicine, Durham, NC, USA 27710

[3] Department of Cell Biology, Duke University School of Medicine, Durham, NC, USA 27710

[4] Department of Microbiology and Immunology, University of North Carolina at Chapel Hill, Chapel Hill, NC, USA 27599

[5] Department of Biomedical Engineering, Duke University Pratt School of Engineering, Durham, NC, USA 27710

[6] Department of Pathology and Laboratory Medicine, Tulane University School of Medicine, New Orleans, LA, USA 70112

Correspondence to:
*Edward A. Miao
Email: edward.miao@duke.edu
Phone: 919-668-7555

Keywords: pyroptosis, apoptosis, *Salmonella*, regulated cell death, extrusion

Abstract

Pyroptosis and apoptosis are two forms of regulated cell death that can defend against intracellular infection. Although pyroptosis and apoptosis have distinct signaling pathways, when a cell fails to complete pyroptosis, backup pathways will initiate apoptosis. Here, we investigated the utility of apoptosis compared to pyroptosis in defense against an intracellular bacterial infection. We previously engineered *Salmonella enterica* serovar Typhimurium to persistently express flagellin, and thereby activate NLRC4 during systemic infection in mice. The resulting pyroptosis clears this flagellin-engineered strain. We now show that infection of caspase-1 or gasdermin D deficient macrophages by this flagellin-engineered *S*. Typhimurium induces apoptosis in vitro. Additionally, we also now engineer *S*. Typhimurium to translocate the pro-apoptotic BH3 domain of BID, which also triggers apoptosis in macrophages in vitro. In both engineered strains, apoptosis occurred somewhat slower than pyroptosis. During mouse infection, the apoptotic pathway successfully cleared these engineered *S.* Typhimurium from the intestinal niche, but failed to clear the bacteria in the myeloid niche in the spleen or lymph nodes. In contrast, the pyroptotic pathway was beneficial in defense of both niches. In order to clear an infection, distinct cell types may have specific tasks (bucket lists) that they must complete before they die. In some cells, either apoptotic or pyroptotic signaling may initiate the same bucket list, whereas in other cell types these modes of cell death may lead to different bucket lists that may not be identical in defense against infection.

Main Text

Introduction

Regulated cell death (RCD) is essential to the survival of a species. There are many reasons why a cell may choose to die, including DNA damage, disruptions to the cell cycle, or detection of an intracellular infection. Subsequently, there are several pathways through which a cell can accomplish RCD, including apoptosis and pyroptosis. These forms of RCD are essential in immune defense against a variety of intracellular pathogens. Failing to accomplish cell death could allow a pathogen to replicate unchecked in a sequestered intracellular niche. On the surface, it might seem that terminating the intracellular replication niche is the most important task for RCD to accomplish. In this case, any modality of RCD should be sufficient to counteract an intracellular infection. That said, apoptosis and pyroptosis have distinct consequences.

Apoptosis is a non-lytic form of RCD that does not inherently cause inflammation. Apoptosis can be initiated via intrinsic or extrinsic signals (Czabotar et al., 2014; Nagata and Tanaka, 2017). The intrinsic pathway is regulated by the BCL-2 family of proteins, which monitor the cell for signs of damage or stress. Cellular stress leads to the activation of the pro-apoptotic subset of this family, called BH3-only proteins (e.g. BID). When these activation signals overcome inhibition by the anti-apoptotic subset of this family (e.g. BCL-2, MCL-1), it leads to assembly of BAK and/or BAX that form pores on mitochondria. The resulting mitochondrial outer membrane permeabilization (MOMP) leads to release of cytochrome *c*. Cytochrome *c* initiates formation of the apoptosome, activating caspase-9, which in turn cleaves and activates caspase-3, the prototypical executioner for apoptosis. Caspase-9 and -3 also activate caspase-7, which can cleave many of the caspase-3 target proteins that drive apoptosis, but whose unique function is to hyperactive membrane repair (Nozaki et al., 2022b). Apoptosis can also be activated by cell-extrinsic pathways through death receptors (e.g. FAS, TNFR1), which in turn leads to activation of caspase-8 (Czabotar et al., 2014; Nagata and Tanaka, 2017). These signaling pathways can reinforce each other, as

caspase-8 can also cleave BID. Caspase-3 then cleaves numerous substrates that together convert a cell into apoptotic bodies.

In contrast, pyroptosis is a lytic, inherently inflammatory form of RCD typically initiated by inflammasomes, which detect signs of infection within the cytosolic compartment. Some inflammasomes directly detect microbial molecules, including proteins, LPS, or DNA; other inflammasomes indirectly detect the cytosolic perturbations caused by toxins (Jorgensen et al., 2017; Nozaki et al., 2022a). For example, NLRC4 can detect the activity of bacterial type III secretion systems when they aberrantly inject flagellin, rod, or needle proteins. These are directly detected via NAIP5/6, NAIP2, and NAIP1, respectively. NLRC4 can signal directly to caspase-1 to initiate pyroptosis, or indirectly via the ASC adaptor. ASC facilitates enhanced caspase-1 activation and is necessary for caspase-1 to efficiently cleave the cytokines pro-IL-1β and pro-IL-18 into their mature forms (Broz et al., 2010b). However, after NLRC4 activation, the direct activation of caspase-1 results in gasdermin D cleavage and activation without a requirement for ASC (Broz et al., 2010b; Kovacs and Miao, 2017). Cleaved gasdermin D then forms a pore on the cell membrane, which is large enough to release mature IL-1β and IL-18 from the cell and to cause pyroptosis (Xia et al., 2021).

While apoptosis and pyroptosis are caused by distinct signaling events, there is nevertheless cross talk between these pathways. For example, there are distinct nodes where pyroptotic signaling proteins can also initiate apoptotic signaling. If downstream pyroptotic signaling is then inhibited, the cell will undergo apoptosis instead. Herein, we refer to these pathways as backup apoptosis. The most apical node is ASC, which can recruit caspase-8 (Pierini et al., 2012). Below this, caspase-1 can activate two different backup apoptosis pathways – by cleaving BID (Guégan et al., 2002; Heilig et al., 2020; Tsuchiya et al., 2019) and by cleaving caspase-7 (Lamkanfi et al., 2008; Mahib et al., 2020). Although we propose that the primary function of caspase-7 is to drive membrane repair (Nozaki et al., 2022b), when it is activated in the absence of pores it might result in a partial form of apoptosis. All of this raises the question: are apoptosis and pyroptosis equal and redundant by simply eliminating the intracellular niche?

Many intracellular bacteria have evolved mechanisms to evade detection by inflammasomes (Jorgensen et al., 2017; Lacey and Miao, 2019; Maltez and Miao, 2016). Therefore, backup apoptosis could restore cell death in the case of bacteria that inhibit pyroptosis (Luchetti et al., 2021). To evade detection by inflammasomes, *Salmonella enterica* serovar Typhimurium encodes two distinct T3SS apparati. The *Salmonella* pathogenicity island 1 (SPI1) T3SS is used to invade epithelial cells. However, the flagellin that is co-expressed is detected by NLRC4, as are the SPI1 rod and needle proteins, albeit less efficiently (Jorgensen et al., 2017; Pereira et al., 2011; Zhang et al., 2015). This detection is protective for the host in a mouse gastroenteritis model by reducing *S*. Typhimurium intracellular burdens (Broz et al., 2010a). Once *S*. Typhimurium has successfully invaded a cell and occupies the *Salmonella*-containing vacuole (SCV), it represses SPI1 and instead expresses SPI2. The SPI2 T3SS evades detection by NLRC4 via mutations on its rod proteins and by repressing flagellin expression. This evasion permits intracellular replication in epithelial cells and macrophages (Broz et al., 2010a).

We previously demonstrated that during this SPI2-driven intracellular phase, *S.* Typhimurium can be engineered to activate NLRC4. This was accomplished by expressing the NLRC4 agonist FliC under a SPI2 promoter, herein called FliC^{ON} (Miao et al., 2011, 2010a). FliC^{ON} *S.* Typhimurium are detected by NLRC4 during the intracellular phase both in vitro and in vivo. This detection results in clearance of FliC^{ON} during systemic mouse infection (Jorgensen et al., 2017; Jorgensen and Miao, 2015; Miao et al., 2010a). This illustrates that the reason why *S.* Typhimurium normally represses flagellin is that pyroptosis is extremely detrimental to the bacterium during intracellular replication. Furthermore, FliC^{ON} *S.* Typhimurium is useful as an experimental tool with which to investigate the effectiveness of pyroptosis in vivo. At the time of our prior publications, the backup apoptotic pathways were not yet discovered (Heilig et al., 2020; Motani et al., 2010; Tsuchiya et

al., 2019). Here, we investigate whether apoptotic pathways can clear engineered *S*. Typhimurium.

Results

FliC^{ON} *S.* Typhimurium activates apoptotic backup pathways in vitro

We first investigated the relative contribution of these backup pathways (Figure 1A) during FliC^{ON} infection by examining in vitro infections in bone marrow-derived macrophages (BMMs) from various knockout mice. We wished to focus on the intracellular SPI2-driven phase of infection. To ensure SPI1-genes were not expressed, we grew *S*. Typhimurium in SPI2 inducing media prior to infection (Miao et al., 2002). As an additional measure, we used *S*. Typhimurium that were deficient for flagellin and SPI1 (*flgC* and *prgH-K*) so that NLRC4 could only be activated by the engineered FliC^{ON} system (Figure 1B). As a negative control, *Nlrc4*$^{-/-}$ BMMs did not activate either pyroptotic or backup apoptotic pathways (Figure 1C-D). *Casp1*$^{-/-}$ BMMs retain the ASC to caspase-8 pathway; and indeed, we observed weak caspase-8, BID, and caspase-3 cleavage at 4 hours post infection (hpi) (Figure 1D), indicating that this pathway is relatively slow. In contrast, *Gsdmd*$^{-/-}$ BMMs remain competent for both the ASC to caspase-8 and the caspase-1 to BID pathways; and indeed, we observed stronger cleavage of BID, caspase-9, and caspase-3 (Figure 1D). We also noticed stronger caspase-8 cleavage in the *Gsdmd*$^{-/-}$ BMMs compared to the *Casp1*$^{-/-}$ BMMs (Figure 1D), perhaps due to the ability of active caspase-3 and -7 to cleave caspase-8, in a feed-forward loop (Inoue et al., 2009; McComb et al., 2019). Further, only *Gsdmd*$^{-/-}$ BMMs displayed release of cytochrome *c* from the mitochondria to the cytosol during infection (Figure 1C), as expected by faster signaling from caspase-1 to BID. Indeed, we also observed cleaved BID (tBID) localization to the mitochondria (Figure 1C). Compared to *Gsdmd*$^{-/-}$ BMMs, *Asc/Gsdmd*$^{-/-}$ BMMs and *Bid/Gsdmd*$^{-/-}$ BMMs had slightly reduced cleavage of caspase-8, -9 and -3 (Figure S1A) as expected due to loss of only one of the two apoptotic pathways in each double knockout. Interestingly, WT BMMs, which are competent for all apoptotic and pyroptotic pathways showed strong cleavage of gasdermin D but only showed weak cleavage of BID and caspase-7, and lacked cleavage of caspase-9 and -3 (Figure 1D, S1A), suggesting that completion of pyroptosis precludes the apoptotic signaling pathway.

We next assessed viability of WT, *Nlrc4*$^{-/-}$, *Casp1*$^{-/-}$, and *Gsdmd*$^{-/-}$ BMMs during FliC^{ON} infection using a lactate dehydrogenase (LDH) assay (Figure 1E, S1B). WT BMMs showed rapid release of LDH consistent with pyroptosis. In accordance with our western blot data (Figure 1C-D), *Nlrc4*$^{-/-}$ BMMs infected with FliC^{ON} did not show toxicity over time (Figure 1E). While *Casp1*$^{-/-}$ BMMs did show weak caspase-3 cleavage by 4-6 hpi (Figure 1D), they do not show much LDH release over the course of 8 hpi (Figure 1E). As before, *Gsdmd*$^{-/-}$ BMMs showed early signs of loss of viability when compared to *Casp1*$^{-/-}$ BMMs (Figure 1E), agreeing with prior publications with different agonists (Doerflinger et al., 2020; Tsuchiya et al., 2019). *Asc/Gsdmd*$^{-/-}$ BMMs and *Bid/Gsdmd*$^{-/-}$ BMMs showed reduced LDH release compared to *Gsdmd*$^{-/-}$ BMMs (Figure 1E, S1C). Vector control infections showed no LDH release over time (Figure S1B-C). These data indicate that the several backup pathways that remain in a *Gsdmd*$^{-/-}$ BMM cause LDH release, albeit slower than pyroptosis.

Finally, we used propidium iodide (PI) and cleaved caspase-3/7 staining to visualize pyroptotic and apoptotic cells in vitro (Figure 1F and S1D-E). As expected, both WT and *Gsdmd*$^{-/-}$ BMMs infected with FliC^{ON} for 4 h showed strong PI staining, whereas neither *Nlrc4*$^{-/-}$ nor *Casp1*$^{-/-}$ BMMs had a high number of PI positive cells (Figure 1F, S1E). Brightfield images of BMMs infected with FliC^{ON} showed clear pyroptotic morphology in WT BMMs, whereas *Gsdmd*$^{-/-}$ BMMs showed clear apoptotic blebbing that co-stained for cleaved caspase-3 (Figure 1F, S1E). These apoptotic bodies are more clearly visualized in the form of a Z-stack (Movie S1, Figure 1G). *Casp1*$^{-/-}$ BMMs cellular morphology showed early signs of rounding but no apoptotic bodies, whereas *Nlrc4*$^{-/-}$ BMMs infected with FliC^{ON} have no difference in cellular morphology from the

controls (Figure 1F, S1D). Therefore, engineered FliC^{ON} *S. Typhimurium* activates the apoptotic backup pathways in vitro in BMMs.

Backup apoptosis fails to clear FliC^{ON} *S. Typhimurium* in the spleen

We next investigated whether the apoptotic backup pathways cleared *S*. Typhimurium during in vivo systemic infection in mice. We used a competitive index infection model (Beuzón and Holden, 2001), where a single mouse is infected with a vector control WT *S*. Typhimurium mixed with FliC^{ON} *S*. Typhimurium at a 1:1 ratio, each marked with a different antibiotic resistance (Figure 2A and S2A-B). FliC^{ON} was progressively cleared in WT mice at a rate of ~ 10-fold per day compared to WT *S.* Typhimurium (Figure 2B-C), consistent with our prior publications that pyroptosis is sufficient to clear FliC^{ON} (Jorgensen et al., 2016b; Miao et al., 2010a). FliC^{ON} was not cleared in *Nlrc4*$^{-/-}$ mice, as expected (Figure 2B, D). However, FliC^{ON} was also not cleared in *Casp1*$^{-/-}$ mice (Figure 2B, E), even though they are sufficient for the ASC to caspase-8 apoptotic backup pathway (Miao et al., 2010a). Furthermore, FliC^{ON} was not cleared in *Gsdmd*$^{-/-}$ mice that retain caspase-1 to BID, caspase-1 to caspase-7, and ASC to caspase-8 backup pathways (Figure 2B, F). Finally, FliC^{ON} was not cleared in *Asc*/*Gsdmd*$^{-/-}$ or *Bid*/*Gsdmd*$^{-/-}$ mice that retain fewer backup pathways (Figure S2C-D). This lack of clearance also held true in a higher dose 10^5 total CFU infection (Figure 2G-H). Therefore, the apoptotic backup pathways are not sufficient to clear either a high or low dose *S.* Typhimurium infection from the spleen when pyroptotic signaling is blocked.

Engineered BID^{ON} *S.* Typhimurium activates apoptosis in vitro

Apoptosis is more commonly activated by intrinsic cellular signaling than backup pathways branching from pyroptosis. To trigger intrinsic apoptosis, we engineered *S.* Typhimurium to directly induce BID-dependent apoptosis. We fused the pro-apoptotic BH3 domain of murine BID to the T3SS secretion signal of SspH1 via an HA tag (Figure 3A). This SspH1-HA-BID^{BH3} protein was expressed from a SPI2 promoter; we refer to these bacteria as BID^{ON} (Figure 3A). The BH3 domain of BID is sufficient to activate BAX/BAK to cause MOMP, which should lead to intrinsic apoptosis (Figure 3B). BID^{ON} bacteria grew normally in LB media (Figure S3A). In WT BMMs, BID^{ON} caused caspase-3 cleavage, while a negative vector control without the BID^{BH3} domain did not (Figure 3C). The weaker HA band in SspH1-HA-BID^{BH3} compared to SspH1-HA could be due to caspase-3 cleaving after aspartates within the HA tag, which can efficiently destroy the HA epitope. The fused SspH1-HA-BID^{BH3} protein is detectable by western blot with both α-HA and α-BID antibodies (Figure 3C-D). Coincidentally, SspH1-HA-BID^{BH3} is similar in length to full length endogenous BID (predicted 21kDa and 20kDa, respectively), and resolved as a thicker band or sometimes as a doublet at ~20kDa (Figure 3D-E, S3B). BID^{ON} induced release of cytochrome *c* from the mitochondria, followed by weak caspase-9 cleavage, resulting in both cleaved caspase-3 and -7, and weak caspase-8 cleavage (Figure 3E-F). As expected, BID^{ON} did not result in cleaved gasdermin D (Figure 3E), indicating that these timepoints are too early to observe the inactivating cleavage of gasdermin D by caspase-3 (Chen et al., 2019). Morphologically, BID^{ON} infected BMMs showed classic apoptotic blebbing between 4-6 hpi (Figure 3G), which is best visualized via a Z-stack (Movie S2, Figure 3H). Therefore, *S.* Typhimurium can be engineered to trigger cell intrinsic apoptosis in vitro in BMMs.

Apoptosis is induced slower than pyroptosis

Above we described two engineered strains, FliC^{ON} and BID^{ON}, which can be used to initiate three different cell death pathways: 1) FliC^{ON} in WT BMMs causes pyroptosis, 2) FliC^{ON} in *Gsdmd*$^{-/-}$ BMMs causes backup apoptosis, and 3) BID^{ON} in WT BMMs causes intrinsic apoptosis. We compared the kinetics and signaling of these three models. We detected gasdermin D cleavage from FliC^{ON} infection in as little as 1-2 hpi (Figure 4A). However, cleaved caspase-3 from FliC^{ON} in *Gsdmd*$^{-/-}$ BMMs was not detected until 3 hpi, and was pronounced only after 4 hpi (Figure 4A). BID^{ON} induced apoptosis slower still, with cleaved caspase-3 only weakly detected at 4 hpi, and not pronounced until 5 or 6 hpi (Figure 4A). The difference between the kinetics of these apoptotic pathways is likely due to efficient detection of FliC by the NAIP/NLRC4 inflammasome,

which has a theoretical sensitivity to detect a single flagellin protein molecule (Hu et al., 2015; Zhang et al., 2015). On the other hand, BID^{BH3} signaling is buffered by cellular BCL family proteins, which are expected to delay the initiation of the BAK/BAX pore.

These kinetics were also apparent visually, as we observed pyroptotic cells in WT BMMs infected with $FliC^{ON}$ at 2 hpi, whereas we did not see any apoptotic blebbing or cleaved caspase-3/7 in *Gsdmd*$^{-/-}$ BMMs infected with $FliC^{ON}$ or BMMs infected with BID^{ON} until 6 hpi (Figure 4B, S4A-B, Movies S1-2). Correspondingly, we observed strong PI staining in WT BMMs infected with $FliC^{ON}$ at both 2 and 6 hpi (Figure 4B, S4B). In contrast, *Gsdmd*$^{-/-}$ BMMs infected with $FliC^{ON}$ showed no PI staining at 2 hpi, and were only PI positive later at 6 hpi. BID^{ON} infected BMMs were similarly delayed, with slightly weaker PI staining (Figure 4B), again consistent with somewhat slower kinetics in the BID^{ON} infection.

Intrinsic apoptosis does not clear engineered *S.* Typhimurium in the spleen
Next, we wanted to determine whether BID^{ON} was cleared in vivo using the competitive index assay. Whereas $FliC^{ON}$ was cleared in WT mice, BID^{ON} was not (Figure 5A-B). $FliC^{ON}$ clearance is progressive over 48 hpi, whereas BID^{ON} burdens increased in ratios equivalent to vector control *S*. Typhimurium over this period (Figure 5B). We also compared our two apoptosis-inducing models, and found that both $FliC^{ON}$ in *Gsdmd*$^{-/-}$ mice and BID^{ON} in WT mice were statistically equal in their lack of clearance (Figure 5C-D).

Pyroptosis is pro-inflammatory, whereas apoptosis itself does not inherently promote inflammation. We hypothesized that specific inflammatory signals such as IL-1β, IL-18, or other cytosolic molecules released by pyroptosis might be required to promote bacterial clearance after RCD. These would be produced during $FliC^{ON}$ infection in WT mice, but should be absent during BID^{ON} infection. To include pyroptosis-induced inflammatory signals during a BID^{ON} infection, we created a triple competitive index model, wherein a single mouse is infected with equal ratios of a vector control, $FliC^{ON}$, and BID^{ON} simultaneously (Figure 5E, S5A-B). We show that even in the presence of $FliC^{ON}$, BID^{ON} is still not cleared from the spleen during a mouse infection (Figure 5F-G). Therefore, $FliC^{ON}$ does not create a proinflammatory environment in the spleen that alters the failure of BID^{ON} to be cleared. This suggests that the ability of RCD to lead to clearance of engineered *S*. Typhimurium is linked to the specific mode of RCD for that host cell.

Pyroptosis clears $FliC^{ON}$ from myeloid cells
In the spleen, *S.* Typhimurium is established to primarily infect macrophages (Salcedo et al., 2001). To validate that clearance after induction of pyroptosis, but not backup apoptosis, was coming from the macrophage compartment, we infected cell-type specific *Casp1*$^{fl/fl}$ mice. We crossed these mice with either *LysM-cre*, which deletes caspase-1 from myeloid cells, or *Mrp8-cre*, which deletes caspase-1 efficiently from neutrophils and does not efficiently delete caspase-1 in monocytes and macrophages (Abram et al., 2014). We compared these cell-type-specific knockouts to caspase-1 sufficient littermate controls. We found that *Casp1*$^{fl/fl}$ *Mrp8-cre* mice retained the ability to clear $FliC^{ON}$, whereas *Casp1*$^{fl/fl}$ *LysM-cre* mice lost the ability to clear $FliC^{ON}$ (Figure 6A-B). This is in contrast to our prior data where we show that caspase-11 within the neutrophil compartment is necessary for clearance of *Burkholderia thailandensis* (Kovacs et al., 2020). Therefore, when macrophages have caspase-1, $FliC^{ON}$ *S.* Typhimurium is successfully cleared from the spleen. However, when caspase-1 is deleted from macrophages, $FliC^{ON}$ is no longer cleared. These data indicate that pyroptosis clears $FliC^{ON}$ from the macrophage compartment, whereas backup apoptosis fails to clear $FliC^{ON}$ from this compartment.

Apoptotic pathways clear engineered *S.* Typhimurium during intestinal infection
The apoptotic backup pathways have previously been shown to successfully clear non-engineered WT *S.* Typhimurium infection downstream of NLRC4 in intestinal epithelial cells (IECs) (Rauch et al., 2017). This is in disagreement with our results above using engineered *S.* Typhimurium during systemic infection in the myeloid compartment of the spleen. Given this, we

decided to test the utility of the apoptotic backup pathways during oral infection. During infection with non-engineered WT *S.* Typhimurium, the bacteria naturally express both flagellin, SPI1 rod, and SPI1 needle in the gut lumen. Among these NLRC4 agonists, flagellin accounts for the vast majority of NLRC4 activation, and SPI1 rod and needle protein are relatively inefficiently detected (Miao et al., 2006). FliC^{ON} engineering does not prevent the bacteria from expressing these endogenous genes. To create an infection model where the majority of NLRC4 activation arises only from the engineered FliC^{ON}, we used a *flgB* mutant background to ablate endogenous flagellin expression and used a competitive index vs vector control bacteria. In the streptomycin-pretreated oral infection model, the IEC compartment can be assessed by examining gentamicin protected bacterial burdens in the cecum (Rauch et al., 2017), and from the same mice the myeloid compartment can be assessed in the draining mesenteric lymph nodes (MLN).

As a control, FliC^{ON} burdens were equal to the vector control within the fecal samples, where no selective pressure should exist (Figure 7A-B). FliC^{ON} was cleared from MLN after oral infection of WT mice (Figure 7A-B), which agrees with our above data from the spleen after intraperitoneal infection. FliC^{ON} was also cleared in the gentamicin-protected cecal compartment in WT mice (Figure 7A-B), suggesting that the pyroptotic pathway leads to clearance from both IEC and macrophage compartments. Surprisingly, when we examined the apoptotic backup pathway by infecting *Gsdmd*$^{-/-}$ mice with FliC^{ON}, we observed different results in the two compartments. There was no clearance of FliC^{ON} in the MLN of *Gsdmd*$^{-/-}$ mice (Figure 7A-B), in agreement again with our data from the spleen. However, FliC^{ON} was cleared in the gentamicin-protected cecal compartment of *Gsdmd*$^{-/-}$ mice with efficiencies that were equal to that seen in WT mice (Figure 7A-B). As a control, *Nlrc4*$^{-/-}$ mice were unable to clear FliC^{ON} *S.* Typhimurium from any compartment (Figure S6A-B). Interestingly, *Casp1*$^{-/-}$ mice that retain only the ASC to caspase-8 backup pathway had reduced clearance of FliC^{ON} *S.* Typhimurium from the cecum (Figure S6A-B). This suggests that the apoptotic backup pathways are specifically useful in IECs, in agreement with the data from Rauch et al., however these same pathways fail in myeloid compartments in the lymph nodes or spleen.

We also investigated BID^{ON} *S.* Typhimurium during oral infection again on a *flgB* background, and found BID^{ON} was also cleared from the cecum (Figure 7C-D). In agreement with our in vitro data showing that BID^{ON}-induced apoptosis is slower and less efficient than the apoptotic backup pathways induced by FliC^{ON} in *Gsdmd*$^{-/-}$ BMMs (Figure 4A), clearance of BID^{ON} in the cecum was less efficient than clearance of FliC^{ON} in *Gsdmd*$^{-/-}$ mice (Figure 7A-D). Interestingly, in the MLN compartment, BID^{ON} appears to have a slight advantage versus the vector control *S.* Typhimurium (Figure 7C-D). This matches a weak, but repeatable trend seen in the splenic compartment in previous infections (Figure 5A-B, S6C-D). Therefore, cell-intrinsic apoptotic pathways can also clear engineered *S.* Typhimurium from the IEC compartment, but not from lymph nodes or the spleen (Figure 7E).

Discussion

There are many, interconnected pathways along which a cell might choose to die. Such backup pathways may be useful in a situation where a pathogen has evolved to inhibit the primary mode of RCD. Here, we demonstrate that pyroptosis and apoptosis are not equivalent in their ability to clear engineered *S*. Typhimurium infection. We hypothesize that clearance after RCD is cell-type-dependent because of what happens both before and after cell death occurs. Once a cell initiates cell death signaling, it “knows” that it will die. However, each cell has distinct goals that it needs to complete before it loses all functional capacity, which we recently proposed to be termed “bucket lists” (Nozaki and Miao, 2023). Successful completion of such bucket lists has beneficial effects after the cell dies. Bucket lists can be different in distinct cell types as well as in different signaling pathways in the same cell type. In the case of *S.* Typhimurium, the bacterium targets two distinct cell types: IECs and macrophages. After an IEC dies, it must ensure that it does not leave behind a hole in the epithelial barrier. The bucket list of an IEC is the same after pyroptotic or apoptotic

signaling is initiated, as both pathways trigger the extrusion program (Rauch et al., 2017). Regardless of the initiating signaling events, an IECs key goal of maintaining barrier integrity after death remains the same. In contrast, a macrophage is not a barrier cell and therefore has no such bucket list task. Instead, in macrophages pyroptosis and apoptosis result in two different bucket lists. Pyroptosis converts a cell into pore-induced intracellular traps (PITs), whereas apoptosis converts a macrophage into apoptotic bodies, which are morphologically and immunologically distinct structures.

The bucket list of an IEC is centered around two goals: to remove the affected IEC from the body meanwhile maintaining epithelial barrier integrity. IECs accomplish both goals via a process called extrusion. After initiating either pyroptotic or apoptotic caspases, rather than immediately undergoing classic "pyroptosis" or "apoptosis", an IEC first disassembles its cytoskeleton, then reassembles an actomyosin contractile ring to squeeze itself out of the monolayer. Neighboring cells simultaneously constrict beneath the dying IEC as it extrudes, maintaining barrier integrity (Blander, 2018). The extruded IEC is thereby shed from the body. Using non-engineered WT *S*. Typhimurium during oral infection, Sellin et al. show that NLRC4 reduces bacterial burdens in the cecum by triggering IEC extrusion (Sellin et al., 2014). Rauch et al. showed that these IECs can extrude via either the pyroptotic or backup apoptotic pathways (Rauch et al., 2017). These conclusions are identical to the conclusion we draw from the FliC^{ON} and BID^{ON} engineered *S.* Typhimurium models. We propose that both pyroptotic signaling via caspase-1 and gasdermin D as well as backup apoptotic signaling via caspases-8/9/3 all converge upon similar bucket list tasks that drive similar IEC extrusion programs. Thus, both pyroptotic and apoptotic pathways are sufficient to reduce both engineered and non-engineered *S.* Typhimurium burdens in the IEC compartment.

More recently, Hausmann et al. showed that this IEC extrusion is not only beneficial to reduce the infected IEC compartment, but also restricts dissemination of *S*. Typhimurium to the draining MLN (Hausmann et al., 2020). This detection only occurred in IECs and not in macrophages in the MLN because non-engineered WT *S*. Typhimurium only expresses flagellin and SPI1 rod/needle during invasion of IECs. After dissemination to macrophages, the non-engineered bacteria have successfully repressed flagellin expression and switched from SPI1 to SPI2 T3SS, thereby evading NLRC4 detection (Hausmann et al., 2020). In contrast, flagellin-engineered FliC^{ON} prevents this evasion, triggering NLRC4-dependent pyroptosis. Using FliC^{ON}, we previously showed that after pyroptosis, the dead macrophage turns into a pore-induced intracellular trap (PIT) that traps *S.* Typhimurium in the cell corpse within which it is subsequently efferocytosed by neutrophils (Jorgensen et al., 2016b, 2016a). Neutrophil ROS is then ultimately responsible for killing FliC^{ON}, as mice deficient in phagocyte oxidase are no longer able to clear FliC^{ON} after pyroptosis (Jorgensen et al., 2016b; Miao et al., 2010a). Therefore, there are at least two tasks on the bucket list of a pyroptotic macrophage: to trap bacteria within the PIT and to recruit neutrophils for efferocytosis. Pyroptosis also has other consequences that have not yet been fully proven to be essential bucket list tasks, including damaging intracellular bacteria (Jorgensen et al., 2016b; Liu et al., 2016; Thurston et al., 2016), releasing cytosolic molecules including nutrients (Kovacs and Miao, 2017), disrupting mitochondrial membranes to produce ROS (de Torre-Minguela et al., 2021; Valenti et al., 2022), and activating NINJ1 to cause membrane rupture (Kayagaki et al., 2021).

Apoptosis in macrophages, on the other hand, has a bucket list that is distinct from that of pyroptosis. An apoptotic macrophage packages itself into smaller apoptotic bodies which are then typically efferocytosed by other macrophages in what is classically an anti-inflammatory manner (Morioka et al., 2019; Poon et al., 2014). This bucket list requires careful disassembly and packaging of the internal cellular contents without losing membrane integrity, while also selectively releasing "find me" and "eat me" signals for the efferocytosing macrophages (Elliott and Ravichandran, 2016; Morioka et al., 2019; Ravichandran, 2011). In situations where our engineered *S.* Typhimurium induce apoptosis, they should be trapped within these apoptotic

bodies (Martin et al., 2012). However, the apoptotic bucket lists tasks fail to clear our engineered *S.* Typhimurium from the macrophage compartment. This failure is not universal to all pathogens, as there is robust evidence that apoptosis successfully leads to clearance of other intracellular bacteria (Martin et al., 2012). For example, non-engineered WT *Listeria monocytogenes* is cleared via apoptosis after cytotoxic T lymphocyte attack (McDougal and Sauer, 2018). Further, *L. monocytogenes* that has been engineered to directly induce intrinsic apoptosis (analogous to our BID^{ON} *S.* Typhimurium) is also cleared in the spleen and liver (Theisen and Sauer, 2017). Backup apoptosis is also successful in reducing bacterial replication in the lung during *Legionella pneumophila* infection (Akhter et al., 2009; Gonçalves et al., 2019). However, these apoptotic backup pathways are not successful in clearing other intracellular bacteria, similar to our results. The ASC to caspase-8 backup pathway was first reported in the context of *Francisella novicida* infection in caspase-1 deficient macrophages (Pierini et al., 2012). While the authors report that both pyroptosis and backup apoptosis limit bacterial replication in vitro, this did not translate to a difference in survival or bacterial burdens in a mouse infection (Pierini et al., 2012). Similarly, *C. violaceum* is cleared from the spleen via pyroptosis in WT mice, but backup apoptosis fails to clear *C. violaceum* in pyroptotic knockout mice (Harvest et al., 2023; Maltez et al., 2015; Nozaki et al., 2022b).

Why did apoptosis fail to clear our engineered *S.* Typhimurium? We speculate that *S.* Typhimurium has virulence strategies that prevent apoptosis from being an effective clearance mechanism. *S.* Typhimurium within apoptotic bodies might infect efferocytosing macrophages, preventing effective clearance analogous to the Trojan Horse from Greek mythology (Giusiano, 2021; Liu et al., 2020; Poon et al., 2014; Saha et al., 2021). Another possibility is the slower kinetics of apoptosis compared to pyroptosis permits bacterial replication before host cell death, and in this regard the longer retention of cytosolic nutrients within the apoptotic body may be beneficial to *S.* Typhimurium. Adaptive immunity may change the consequences of apoptosis for *S.* Typhimurium in the macrophage compartment. Indeed, Doerflinger et al. used Δ*aroA S*. Typhimurium at 3 weeks post-infection and saw beneficial utility of apoptotic signaling in clearing the bacteria (Doerflinger et al., 2020). However, our findings show that apoptotic engineering fails to drive innate immune clearance against *S*. Typhimurium within macrophages.

Here we show that clearance of engineered *S*. Typhimurium after RCD is dependent upon the cellular compartment. Pyroptotic signaling leads to rapid clearance of engineered *S*. Typhimurium from both the intestinal and myeloid compartments, while apoptotic signaling leads to clearance only within the intestinal compartment (Figure 7E). Within IECs, pyroptotic and apoptotic signaling lead to the same extrusion bucket list, and therefore are equally sufficient in clearing both engineered and non-engineered *S*. Typhimurium (Rauch et al., 2017). Within macrophages, pyroptotic and apoptotic signaling lead to different bucket lists, and only the pyroptotic bucket list results in clearance of engineered *S*. Typhimurium. However, this is largely evaded by non-engineered WT *S.* Typhimurium, which successfully replicate in macrophages (Hausmann et al., 2020; Miao et al., 2010a, 2010b; Salcedo et al., 2001). Therefore, we propose that it is the correct cellular bucket list in the context of each specific cell type, rather than simply the type of RCD, that ultimately leads to clearance of intracellular bacteria.

Materials and Methods

Plasmid Construction

pTA007 (BID^{ON}) was created by fusing the BH3 domain of murine BID (AA79-102) to the *S.* Typhimurium T3SS secretion signal of SspH1(AA1-137) via an HA tag. This fused SspH1-HA-$mBID^{BH3}$ was put under the control of *sseJ* promotor and inserted into pWSK29. pTA021 (SspH1-HA) was created using the same strategy as pTA007, but did not include the murine BID^{BH3} domain. pTA015 ($FliC^{ON}$ (kan)) was created by digesting P_{sseJ}-*fliC-fliS* from $FliC^{ON}$ and inserting

the fragment into pWSK129. pTA016 (BID^{ON} (kan)) was created by digesting the P_{sseJ}-*sspH1-HA-BID^{BH3}* from BID^{ON} and inserting into pWSK129. pWSK229 was created by replacing the ampicillin resistance cassette of pWSK29 with a chloramphenicol resistance cassette cloned from pTwist Chlor MC from Twist Biosciences.

Bacterial Strains and Culture Conditions

All *Salmonella enterica* serovar Typhimurium strains were derived from ATCC 14028s or SL1344. In vivo systemic infections were performed in 14028s with the indicated plasmids. In vivo oral infections were performed in SL1344 on a *flgB* mutant background with the indicated plasmids. In vitro infections were performed using Δ*flgC ΔprgH-K S*. Typhimurium on the CS401 derivative of 14028s (used for the genetic deletion system) to eliminate flagellin and SPI1 T3SS expression from chromosomal loci. To eliminate flagellin expression from chromosomal loci during mouse infections, Δ*flgB* 14028s *S*. Typhimurium were used for Figure 2G-H and 2 of 3 replicates of Figure 5A-B. However, we found that experimental results were identical using wild-type *S*. Typhimurium, therefore wild type 14028s *S*. Typhimurium were used for all other systemic mouse infections. Plasmids are listed in Table 1. All strains were grown in 2mL Miller's LB Broth (Apex Bioresearch Products, Cat. 11-120) with appropriate antibiotics overnight at 37°C with aeration. For the growth curve, a 1:1000 dilution of overnight culture into 50 ml LB broth was put at 37°C with aeration. A 1 ml sample was removed and OD600 analyzed via spectrophotometer every hour until growth stabilized. An OD600 of 1 ≈ $1x10^9$ CFU was used.

Table 1. Plasmids

Plasmids	Alias	Resistance	Notes	Reference
pWSK29	Vector	Amp	Low copy vector	(Rong Fu Wang and Kushner, 1991)
pWSK129	Vector	Kan	Low copy vector	(Rong Fu Wang and Kushner, 1991)
pDM1	$FliC^{ON}$	Amp	pWSK29 expressing *fliC fliS* from *sseJ* promotor	(Miao et al., 2010a)
pTA007	BID^{ON} or BID^{ON} (amp)	Amp	pWSK29 expressing *sspH1-HA-$mBID^{BH3}$* from *sseJ* promotor	This work
pTA021	sspH1-HA	Amp	pWSK29 expressing *sspH1-HA* from *sseJ* promotor	This work
pWSK229	Vector	Cam	Low copy vector	This work
pTA015	$FliC^{ON}$ (kan)	Kan	pWSK129 expressing *fliC fliS* from *sseJ* promotor	This work
pTA016	BID^{ON} (kan)	Kan	pWSK129 expressing *sspH1-HA-$mBID^{BH3}$* from *sseJ* promotor	This work

Macrophage culture and infection

BMMs were isolated as described (Gonçalves and Mosser, 2015). BMM media consisted of DMEM (Thermo Fisher Cat. 11995073) with 10% FBS and 15% LCM or 10ng/ml M-CSF. Penicillin and streptomycin were added to the media during differentiation and thawing but withheld during seeding and infection. Δ*flgC ΔprgH-K S*. Typhimurium were induced to express SPI2 by back diluting an overnight culture to OD600=0.026 in 3mL SPI2-inducing media, then grown 16-20h in a 37°C shaker (Miao et al., 2002). SPI2-induced bacteria were washed once with PBS prior to calculating MOI. For all BMM infections, "Vector" control is pWSK29. Macrophages were infected with MOI 25, centrifuged for 5 min at 200x*g*, incubated for 1 h, then gentamicin (30µg/ml) was added to the medium to kill any extracellular bacteria. Lipopolysaccharide (50ng/ml) was added to normalize TLR activation for mock infected cells.

Western Blot Analysis

For whole-cell lysates, macrophages were seeded at $2x10^5$ cells/well in 24 well tissue culture treated plates the day before infection. Macrophages infected as described above. At indicated

timepoints, media was aspirated, and 60 µl 1x Laemmli Sample Buffer was added to lyse the cells. Samples were boiled for 5 min at 95°C and frozen at -80°C until analyzed. 12 µl sample was loaded into a 4-12% polyacrylamide TGX Stain-Free gel (Bio-Rad Cat. 4568086) and run for 1 h 15 min at 15mA per gel. Gel was UV activated in order to visualize total protein. Protein was then transferred onto a 0.45 µm PVDF membrane (Millipore, Cat. IPFL85R), blocked with 5% non-fat dried milk in TBS plus 0.01% Tween (TBST) for one hour at room temperature, and incubated overnight at 4°C with mild agitation in 5% milk in TBST plus indicated antibody: cytochrome *c* (1:750, rabbit, Cell Signaling Technology, Cat. 11940), GAPDH (1:10000, rabbit, abcam, Cat. Ab9485), VDAC (1:750, rabbit, Cell Signaling Technology, Cat. 4661), cleaved caspase-8 (1:1000, rabbit, Cell Signaling Technology, Cat. 8592), BID (1:500, rat, R&D Systems, Cat. MAB860), caspase-9 (1:750, mouse, Cell Signaling Technology, Cat. 9508), cleaved caspase-7 (1:1000, rabbit, Cell Signaling Technology, Cat. 9491), cleaved caspase-3 (1:750, rabbit, Cell Signaling Technology, Cat. 9661), gasdermin D (1:1000, rabbit, abcam, Cat. ab209845), or HA (1:2000, mouse, Biolegend, Cat. MMS-101R). Membranes were incubated for 1 h at room temperature with appropriate secondary antibodies: goat anti-rabbit (1:2000, Cell Signaling Technology, Cat. 7074), goat anti-rat (1:10000, Jackson ImmunoResearch, Cat. 112-035-062), or goat anti-mouse (1:10000, Jackson ImmunoResearch, Cat. 115-035-062). ECLs used include ThermoFisher Scientific Pierce ECL (Cat. 32106), SuperSignal West Pico PLUS (Cat. 34580), and SuperSignal West Femto (Cat. 34095). Images taken using an Azure 500 Infrared Imaging System. For cell lysates, blots were probed in the following order: cleaved caspase-3, cleaved caspase-7, cleaved caspase-8, caspase-9, gasdermin D, BID, HA. For cytosolic and mitochondrial fractions, blots were probed in the following order: cytochrome *c*, VDAC, GAPDH, BID. Blots were stripped using a mild stripping buffer protocol ("Western blot membrane stripping for restaining protocol | Abcam," n.d.), then re-blocked with 5% milk. The p43 fragment of cleaved caspase-8 did not always fully strip in the apoptotic signaling conditions, leading to a faint p43 fragment seen in the gasdermin D blot even in *Gsdmd*$^{-/-}$ BMMs. Therefore, we do not believe this faint fragment represents an inactivating cleavage event of gasdermin D by caspse-3.

Cytosolic and Mitochondrial Fraction Isolation

Macrophages were seeded at 1x10^6 cells/well in 6-well non-TC treated plates (Genesee Scientific, Cat. 25-100). Cells were infected as described above. At indicated timepoints, media was aspirated off and cells were lifted using 1 ml PBS + 1 mM EDTA. Cells were spun down and washed 2x with sterile PBS at 300x*g* for 5 min. Cell pellets were permeabilized in 30 µl MOMP buffer (20 mM HEPES pH 7.4, 250 mM sucrose, 1 mM EDTA, 75 mM KCL, 2.5 mM $MgCl_2$, 0.05% digitonin) for 5 minutes on ice. Samples then spun at 15,000x*g* for 10 min at 4°C. Supernatant was collected as "cytosolic" fraction. The pellet washed once in 30 µl PBS, and spun down again at 15,000x*g* for 10 min at 4°C. Wash was discarded, and pellets lysed in 30 µl RPIA buffer on ice for 20 min. Samples spun final time at 18,000x*g* for 10 min at 4°C, and supernatant collected as "mitochondrial" fraction. 10 µl of 4x Laemmeli's Sample Buffer was added per sample, and then boiled at 95°C for 5 min. Samples frozen at -80°C until analyzed by SDS-PAGE and Western blot, described above. Protocol adapted from (Mahajan et al., 2014).

Cytotoxicity Assay

Macrophages were seeded at 5x10^4 cells/well in 96-well TC treated plate. Cells were infected as described above. Supernatant was collected at indicated timepoints and frozen at -80°C until analyzed. Cytotoxicity was determined by lactate dehydrogenase assay (CytoTox 96, Promega, Cat. G1780). All samples and reagents were brought to room temperature before analyzing.

Immunofluorescence and live cell microscopy

For microscopy experiments, bone marrow derived macrophages were plated on 8 well chamber coverslips (Nalge Nunc International, Cat. 155409) at a density of 2.85*10^5 cells / cm^2. At the time of adding gentamicin 1 hour after initiating infection, the following immunofluorescent dyes were added. Dyes were used at the following concentrations: Hoechst 33342 at 2 µg/ml

(ThermoFisher, Cat. H3570), Propidium Iodide at 1 µg/ml (Sigma-Aldrich, Cat. P4864), and NucView-488 at 5 µM (Biotium, Cat. 10402). NucView-488 was selected to visualize activation of Caspase-3 in apoptosis, and Caspase-7 via Caspase-1 in pyroptosis. Images were captured using a Keyence BZ-X810 All-in-One Fluorescence Microscope using 20x and 60x objectives. For 20x image stitching, 15 fields were captured and stitched using BZ-X800 Image Analyzer 1.1.1.8 software.

Mice and Mouse Infections

All mouse strains were bred and housed at Duke University in a pathogen-specific free facility. For infection mice were transferred to a BSL2 infection facility within Duke University, and mice allowed to acclimate for at least two days prior to infection. Wild type C57BL/6J (Jackson Laboratory #000664), *Mrp8-cre* (Jackson Laboratory #021614), *LysM-cre* (Jackson Laboratory #004781), *Casp1*$^{fl/fl}$ (Hu et al., 2016), *Casp1*$^{-/-}$ *Casp11*$^{129mt/129mt}$ (referred to as *Casp1/11*$^{-/-}$) (Kuida et al., 1995), *Gsdmd*$^{-/-}$ (Rauch et al., 2017), *Nlrc4*$^{-/-}$ (Mariathasan et al., 2004), *Casp1*$^{-/-}$ (Rauch et al., 2017), *Bid*$^{-/-}$ (Yin et al., 1999), *Il1b*/*Il18*$^{-/-}$ (Shornick et al., 1996; Takeda et al., 1998). *Asc*$^{-/-}$*Gsdmd*$^{-/-}$ (referred to as *Asc*/*Gsdmd*$^{-/-}$) were created by crossing *Asc*$^{-/-}$ (Mariathasan et al., 2004) and *Gsdmd*$^{-/-}$ mice together. *Bid*$^{-/-}$*Gsdmd*$^{-/-}$ (referred to as *Bid*/*Gsdmd*$^{-/-}$) were created by crossing *Bid*$^{-/-}$ and *Gsdmd*$^{-/-}$ mice together. Animal protocols were approved by the Institutional Animal Care and Use Committee (IACUC) at the University of North Carolina at Chapel Hill or by the IACUC at Duke University and met guidelines of the US National Institutes of Health for the humane care of animals.

For competitive index infections, inoculum was composed equally of the vector control (pWSK129) and experimental strain (FliC^{ON} or BID^{ON}, as indicated). For triple competitive index, the inoculum was composed equally of $5x10^2$ vector control (pWSK229), FliC^{ON} (kan), and BID^{ON} for $1.5x10^3$ total CFU. For systemic infection, mice were infected intraperitoneally with a total of $1x10^3$ (low dose) or $1x10^5$ (high dose) *S*. Typhimurium. Spleens were harvested at indicated timepoints and homogenized in a 2ml homogenizer tube (Fisher Brand Cat. 14-666-315) containing 1ml sterile PBS and one 5mm stainless steel bead (QIAGEN Cat. 69989). For oral infection, mice were first fasted for 4 hours and then orally inoculated with 20mg of streptomycin sulfate (Sigma Cat. 59137) which was filter sterilized using 0.22µm filter (Genesee Cat. 25-244). The next day, mice were again fasted for 4 hours and then orally infected with a total of $1x10^7$ *S*. Typhimurium. Food was returned 2 hours post infection. At 48 hpi, the cecum, mesenteric lymph nodes, and a fecal sample were isolated. The fecal sample was homogenized under the same condition as spleens, described above. The MLN was homogenized using a 2mL homogenizer tube (OMBI International Cat. 19-649) containing 1ml sterile PBS and 7-10 2.4mm stainless steel beads (OMBI International Cat. 19-640-3). The cecum was first washed in PBS, then incubated on a room temperature rocker at 25 rpm in 400ug/ml gentamycin (ThermoFisher Cat. 15750060) for 30 min, then washed in fresh PBS for another 30 min. Caeca were then homogenized under the same conditions as MLNs. Spleens and fecal samples homogenized using a Retsch MM400 homogenizer for 5 min at 30Hz. Fecal samples were spun down for 30 s and 5000 rpm after homogenizing. Cecum and MLNs were homogenized using a Fisherbrand Bead Mill 24 homogenizer for at speed 4 for 4 cycles of 1 min homogenizing with 30 s dwell time. After homogenization, lysates were serially diluted 1:5 in sterile PBS and plated on LB plates containing appropriate antibiotics. Plates were incubated overnight at 37°C and colony forming units counted. Competitive index results are presented as vector CFU/experimental CFU, normalized to ratio of plated inoculum.

Statistics

All statistical analysis was performed with GraphPad Prism 9. Discrete data was first assessed for normal distribution using a Shapiro-Wilk normality test. Data with normal distribution was analyzed with either unpaired two-tail t test (2 groups) or a one-way ANOVA (3 or more groups). Discrete data that did not have a normal distribution was analyzed with a Mann-Whitney (2 groups) or Kruskal-Wallis (3 or more groups). Experiments with two factors were analyzed with a two-way ANOVA.

Data, Materials, and Software Availability
All study data are included in the article and have been uploaded LabArchives. Plasmid maps of novel constructs will be made available upon request and have been saved in Benchling.

Acknowledgments
We thank Richard Flavell, Russell Vance, and Vishva Dixit for sharing mice. This work is supported by NIH grants AI133236, AI139304, AI136920 (E.A.M.), and AI133236-04S1(C.K.H), and the National Science Foundation Graduate Research Fellowship Program DGE 2139754 (T.J.A.). Any opinions, findings, and conclusions or recommendations expressed in this material are those of the author(s) and do not necessarily reflect the views of the National Science Foundation. Figure 7E created with BioRender.com under agreement number GZ25BXK3N9.

Author Contributions: T.J.A. led the project and performed most of the experiments. Z.P.B., L.L., C.K.H., and A.K.B. performed some experiments. G.R.M. and J.P.L. initiated the project. H.N.L. managed the mouse colony. X.Y. provided BID expertise. T.J.A. and E.A.M. wrote the paper. E.A.M. oversaw the project.

Competing Interest Statement: Authors declare no competing interests.

References

Abram CL, Roberge GL, Hu Y, Lowell CA. 2014. Comparative analysis of the efficiency and specificity of myeloid-Cre deleting strains using ROSA-EYFP reporter mice. *J Immunol Methods* **408**:89–100. doi:10.1016/J.JIM.2014.05.009

Akhter A, Gavrilin MA, Frantz L, Washington S, Ditty C, Limoli D, Day C, Sarkar A, Newland C, Butchar J, Marsh CB, Wewers MD, Tridandapani S, Kanneganti TD, Amer AO. 2009. Caspase-7 Activation by the Nlrc4/Ipaf Inflammasome Restricts Legionella pneumophila Infection. *PLoS Pathog* **5**:e1000361. doi:10.1371/JOURNAL.PPAT.1000361

Beuzón CR, Holden DW. 2001. Use of mixed infections with Salmonella strains to study virulence genes and their interactions in vivo. *Microbes Infect* **3**:1345–1352. doi:10.1016/S1286-4579(01)01496-4

Blander JM. 2018. On cell death in the intestinal epithelium and its impact on gut homeostasis. *Curr Opin Gastroenterol* **34**:413–419. doi:10.1097/MOG.0000000000000481

Broz P, Newton K, Lamkanfi M, Mariathasan S, Dixit VM, Monack DM. 2010a. Redundant roles for inflammasome receptors NLRP3 and NLRC4 in host defense against Salmonella. *Journal of Experimental Medicine* **207**:1745–1755. doi:10.1084/jem.20100257

Broz P, Von Moltke J, Jones JW, Vance RE, Monack DM. 2010b. Differential requirement for Caspase-1 autoproteolysis in pathogen-induced cell death and cytokine processing. *Cell Host Microbe* **8**:471. doi:10.1016/J.CHOM.2010.11.007

Chen KW, Demarco B, Heilig R, Shkarina K, Boettcher A, Farady CJ, Pelczar P, Broz P. 2019. Extrinsic and intrinsic apoptosis activate pannexin-1 to drive NLRP3 inflammasome assembly. *EMBO J* **38**. doi:10.15252/embj.2019101638

Czabotar PE, Lessene G, Strasser A, Adams JM. 2014. Control of apoptosis by the BCL-2 protein family: implications for physiology and therapy. *Nat Rev Mol Cell Biol*. doi:10.1038/nrm3722

de Torre-Minguela C, Gómez AI, Couillin I, Pelegrín P. 2021. Gasdermins mediate cellular release of mitochondrial DNA during pyroptosis and apoptosis. *FASEB J* **35**. doi:10.1096/FJ.202100085R

Doerflinger M, Deng Y, Whitney P, Salvamoser R, Engel S, Kueh AJ, Tai L, Bachem A, Gressier E, Geoghegan ND, Wilcox S, Rogers KL, Garnham AL, Dengler MA, Bader SM, Ebert G, Pearson JS, De Nardo D, Wang N, Yang C, Pereira M, Bryant CE, Strugnell RA, Vince JE, Pellegrini M, Strasser A, Bedoui S, Herold MJ. 2020. Flexible Usage and Interconnectivity of Diverse Cell Death Pathways Protect against Intracellular Infection. *Immunity* 1–15. doi:10.1016/j.immuni.2020.07.004

Elliott MR, Ravichandran KS. 2016. The Dynamic of Apoptotic Cell Clearance. *Dev Cell* **38**:147–160. doi:.1037//0033-2909.I26.1.78

Giusiano G. 2021. The Trojan Horse Model in Paracoccidioides: A Fantastic Pathway to Survive Infecting Human Cells. *Front Cell Infect Microbiol* **10**. doi:10.3389/FCIMB.2020.605679

Gonçalves R, Mosser DM. 2015. The Isolation and Characterization of Murine Macrophages. *Curr Protoc Immunol* **111**:14.1.1-14.1.16. doi:10.1002/0471142735.IM1401S111

Gonçalves A V., Margolis SR, Quirino GFS, Mascarenhas DPA, Rauch I, Nichols RD, Ansaldo E, Fontana MF, Vance RE, Zamboni DS. 2019. Gasdermin-D and caspase-7 are the key caspase-1/8 substrates downstream of the NAIP5/NLRC4 inflammasome required for restriction of legionella pneumophila. *PLoS Pathog* **15**. doi:10.1371/journal.ppat.1007886

Guégan C, Vila M, Teissman P, Chen C, Onténiente B, Li M, Friedlander RM, Przedborski S. 2002. Instrumental Activation of Bid by Caspase-1 in a Transgenic Mouse Model of ALS. *Molecular and Cellular Neuroscience* **20**:533–562. doi:10.1006/mcne.2002.1136

Harvest CK, Abele TJ, Yu C, Beatty CJ, Amason ME, Billman ZP, DePrizio MA, Lacey CA, Maltez VI, Larson HN, McGlaughon BD, Saban DR, Montgomery SA, Miao EA. 2023. An innate granuloma eradicates an environmental pathogen using Gsdmd and Nos2. *bioRxiv* 2023.03.07.531568. doi:10.1101/2023.03.07.531568

Hausmann A, Böck D, Geiser P, Berthold DL, Fattinger SA, Furter M, Bouman JA, Barthel-Scherrer M, Lang CM, Bakkeren E, Kolinko I, Diard M, Bumann D, Slack E, Regoes RR, Pilhofer M, Sellin ME, Hardt WD. 2020. Intestinal epithelial NAIP/NLRC4 restricts systemic dissemination of the adapted pathogen Salmonella Typhimurium due to site-specific bacterial PAMP expression. *Mucosal Immunol* **13**:530–544. doi:10.1038/S41385-019-0247-0

Heilig R, Dilucca M, Boucher D, Chen KW, Hancz D, Demarco B, Shkarina K, Broz P. 2020. Caspase-1 cleaves Bid to release mitochondrial SMAC and drive secondary necrosis in the absence of GSDMD. *Life Sci Alliance* **3**:1–15. doi:10.26508/LSA.202000735

Hu B, Jin C, Li HB, Tong J, Ouyang X, Cetinbas NM, Zhu S, Strowig T, Lam FC, Zhao C, Henao-Mejia J, Yilmaz O, Fitzgerald KA, Eisenbarth SC, Elinav E, Flavell RA. 2016. The DNA Sensing Aim2 Inflammasome Controls Radiation Induced Cell death and Tissue Injury. *Science* **354**:765. doi:10.1126/SCIENCE.AAF7532

Hu Z, Zhou Q, Zhang C, Fan S, Cheng W, Zhao Y, Shao F, Wang HW, Sui SF, Chai J. 2015. Structural and biochemical basis for induced self-propagation of NLRC4. *Science (1979)* **350**:399–404. doi:10.1126/SCIENCE.AAC5489/SUPPL_FILE/PAPV2.PDF

Inoue S, Browne G, Melino G, Cohen GM. 2009. Ordering of caspases in cells undergoing apoptosis by the intrinsic pathway. *Cell Death & Differentiation 2009 16:7* **16**:1053–1061. doi:10.1038/cdd.2009.29

Jorgensen I, Lopez JP, Laufer SA, Miao EA. 2016a. IL-1β, IL-18, and eicosanoids promote neutrophil recruitment to pore-induced intracellular traps following pyroptosis. *Eur J Immunol* **46**:2761–2766. doi:10.1002/eji.201646647

Jorgensen I, Miao EA. 2015. Pyroptotic cell death defends against intracellular pathogens. *Immunol Rev* **265**:130–142. doi:10.1111/imr.12287

Jorgensen I, Rayamajhi M, Miao EA. 2017. Programmed cell death as a defence against infection. *Nat Rev Immunol* **17**:151–164. doi:10.1038/nri.2016.147

Jorgensen I, Zhang Y, Krantz BA, Miao EA. 2016b. Pyroptosis triggers pore-induced intracellular traps (PITs) that capture bacteria and lead to their clearance by efferocytosis. *Journal of Experimental Medicine* **213**:2113–2128. doi:10.1084/jem.20151613

Kayagaki N, Kornfeld OS, Lee BL, Stowe IB, O'Rourke K, Li Q, Sandoval W, Yan D, Kang J, Xu M, Zhang J, Lee WP, McKenzie BS, Ulas G, Payandeh J, Roose-Girma M, Modrusan Z, Reja R, Sagolla M, Webster JD, Cho V, Andrews TD, Morris LX, Miosge LA, Goodnow CC, Bertram EM, Dixit VM. 2021. NINJ1 mediates plasma membrane rupture during lytic cell death. *Nature* **591**:131–136. doi:10.1038/S41586-021-03218-7

Kovacs SB, Miao EA. 2017. Gasdermins: Effectors of Pyroptosis. *Trends Cell Biol* **27**:673–684. doi:10.1016/j.tcb.2017.05.005

Kovacs SB, Oh C, Maltez VI, McGlaughon BD, Verma A, Miao EA, Aachoui Y. 2020. Neutrophil Caspase-11 Is Essential to Defend against a Cytosol-Invasive Bacterium. *Cell Rep* **32**:107967. doi:10.1016/j.celrep.2020.107967

Kuida K, Lippke JA, Ku G, Harding MW, Livingston DJ, Su MSS, Flavell RA. 1995. Altered Cytokine Export and Apoptosis in Mice Deficient in Interleukin-1β Converting Enzyme. *Science (1979)* **267**:2000–2003. doi:10.1126/SCIENCE.7535475

Lacey CA, Miao EA. 2019. Programmed Cell Death in the Evolutionary Race against Bacterial Virulence Factors. *Cold Spring Harb Perspect Biol* a036459. doi:10.1101/cshperspect.a036459

Lamkanfi M, Kanneganti TD, van Damme P, vanden Berghe T, Vanoverberghe I, Vandekerckhove J, Vandenabeele P, Gevaert K, Núñe-az G. 2008. Targeted Peptidecentric Proteomics Reveals Caspase-7 as a Substrate of the Caspase-1 Inflammasomes. *Mol Cell Proteomics* **7**:2350. doi:10.1074/MCP.M800132-MCP200

Liu X, Zhang Z, Ruan J, Pan Y, Magupalli VG, Wu H, Lieberman J. 2016. Inflammasome-activated gasdermin D causes pyroptosis by forming membrane pores. *Nature* **535**:153–158. doi:10.1038/NATURE18629

Liu Y, Jia Y, Yang K, Wang Z. 2020. Heterogeneous Strategies to Eliminate Intracellular Bacterial Pathogens. *Front Microbiol* **11**. doi:10.3389/FMICB.2020.00563

Luchetti G, Roncaioli JL, Chavez RA, Schubert AF, Kofoed EM, Reja R, Cheung TK, Liang Y, Webster JD, Lehoux I, Skippington E, Reeder J, Haley B, Tan MW, Rose CM, Newton K, Kayagaki N, Vance RE, Dixit VM. 2021. Shigella ubiquitin ligase IpaH7.8 targets Gasdermin D for degradation to prevent pyroptosis and enable infection. *Cell Host Microbe* **29**:1521. doi:10.1016/J.CHOM.2021.08.010

Mahajan IM, Chen M Der, Muro I, Robertson JD, Wright CW, Bratton SB. 2014. BH3-Only Protein BIM Mediates Heat Shock-Induced Apoptosis. *PLoS One* **9**:84388. doi:10.1371/JOURNAL.PONE.0084388

Mahib MR, Hosojima S, Kushiyama H, Kinoshita T, Shiroishi T, Suda T, Tsuchiya K. 2020. Caspase-7 mediates caspase-1-induced apoptosis independently of Bid. *Microbiol Immunol* **64**:143–152. doi:10.1111/1348-0421.12756

Maltez VI, Miao EA. 2016. Reassessing the Evolutionary Importance of Inflammasomes. *The Journal of Immunology* **196**:956–962. doi:10.4049/jimmunol.1502060

Maltez VI, Tubbs AL, Cook KD, Aachoui Y, Falcone EL, Holland SM, Whitmire JK, Miao EA. 2015. Inflammasomes Coordinate Pyroptosis and Natural Killer Cell Cytotoxicity to Clear Infection by a Ubiquitous Environmental Bacterium. *Immunity* **43**:987–997. doi:10.1016/j.immuni.2015.10.010

Mariathasan S, Hewton K, Monack DM, Vucic D, French DM, Lee WP, Roose-Girma M, Erickson S, Dixit VM. 2004. Differential activation of the inflammasome by caspase-1 adaptors ASC and Ipaf. *Nature 2004 430:6996* **430**:213–218. doi:10.1038/nature02664

Martin CJ, Booty MG, Rosebrock TR, Nunes-Alves C, Desjardins DM, Keren I, Fortune SM, Remold HG, Behar SM. 2012. Efferocytosis is an innate antibacterial mechanism. *Cell Host Microbe* **12**:289–300. doi:10.1016/j.chom.2012.06.010

McComb S, Chan PK, Guinot A, Hartmannsdottir H, Jenni S, Dobay MP, Bourquin JP, Bornhauser BC. 2019. Efficient apoptosis requires feedback amplification of upstream apoptotic signals by effector caspase-3 or -7. *Sci Adv* **5**:9433–9464. doi:10.1126/SCIADV.AAU9433

McDougal CE, Sauer JD. 2018. Listeria monocytogenes: The impact of cell death on infection and immunity. *Pathogens* **7**. doi:10.3390/pathogens7010008

Miao EA, Alpuche-Aranda CM, Dors M, Clark AE, Bader MW, Miller SI, Aderem A. 2006. Cytoplasmic flagellin activates caspase-1 and secretion of interleukin 1β via Ipaf. *Nat Immunol* **7**:569–575. doi:10.1038/ni1344

Miao EA, Freeman JA, Miller SI. 2002. Transcription of the SsrAB Regulon Is Repressed by Alkaline pH and Is Independent of PhoPQ and Magnesium Concentration. *J Bacteriol* **184**:1493. doi:10.1128/JB.184.5.1493-1497.2002

Miao EA, Leaf IA, Treuting PM, Mao DP, Dors M, Sarkar A, Warren SE, Wewers MD, Aderem A. 2010a. Caspase-1-induced pyroptosis is an innate immune effector mechanism against intracellular bacteria. *Nat Immunol*. doi:10.1038/ni.1960

Miao EA, Mao DP, Yudkovsky N, Bonneau R, Lorang CG, Warren SE, Leaf IA, Aderem A. 2010b. Innate immune detection of the type III secretion apparatus through the NLRC4 inflammasome. *Proc Natl Acad Sci U S A* **107**:3076–3080. doi:10.1073/PNAS.0913087107

Miao EA, Rajan J V., Aderem A. 2011. Caspase-1-induced pyroptotic cell death. *Immunol Rev* **243**:206–214. doi:10.1111/j.1600-065X.2011.01044.x

Morioka S, Maueröder C, Ravichandran KS. 2019. Living on the Edge: Efferocytosis at the Interface of Homeostasis and Pathology. *Immunity* **50**:1149–1162. doi:10.1016/j.immuni.2019.04.018

Motani K, Kawase K, Imamura R, Kinoshita T, Kushiyama H, Suda T. 2010. Activation of ASC induces apoptosis or necrosis, depending on the cell type, and causes tumor eradication. *Cancer Sci* **101**:1822–1827. doi:10.1111/J.1349-7006.2010.01610.X

Nagata S, Tanaka M. 2017. Programmed cell death and the immune system. *Nat Rev Immunol* **17**:333–340. doi:10.1038/nri.2016.153

Nozaki K, Li L, Miao EA. 2022a. Innate Sensors Trigger Regulated Cell Death to Combat Intracellular Infection. *Annu Rev Immunol* **40**:469–498. doi:10.1146/ANNUREV-IMMUNOL-101320-011235

Nozaki K, Maltez VI, Rayamajhi M, Tubbs AL, Mitchell JE, Lacey CA, Harvest CK, Li L, Nash WT, Larson HN, McGlaughon BD, Moorman NJ, Brown MG, Whitmire JK, Miao EA. 2022b. Caspase-7 activates ASM to repair gasdermin and perforin pores. *Nature 2022* 1–8. doi:10.1038/s41586-022-04825-8

Nozaki K, Miao EA. 2023. Bucket lists must be completed during cell death. *Trends Cell Biol*. doi:10.1016/J.TCB.2023.02.008

Pereira MSF, Morgantetti GF, Massis LM, Horta C V., Hori JI, Zamboni DS. 2011. Activation of NLRC4 by Flagellated Bacteria Triggers Caspase-1–Dependent and –Independent Responses To Restrict Legionella pneumophila Replication in Macrophages and In Vivo. *The Journal of Immunology* **187**:6447–6455. doi:10.4049/JIMMUNOL.1003784

Pierini R, Juruj C, Perret M, Jones CL, Mangeot P, Weiss DS, Henry T. 2012. AIM2/ASC triggers caspase-8-dependent apoptosis in Francisella-infected caspase-1-deficient macrophages. *Cell Death & Differentiation 2012 19:10* **19**:1709–1721. doi:10.1038/cdd.2012.51

Poon IKH, Lucas CD, Rossi AG, Ravichandran KS. 2014. Apoptotic cell clearance: basic biology and therapeutic potential. *Nat Rev Immunol* **14**:166–180. doi:10.1038/nri3607

Rauch I, Deets KA, Ji DX, von Moltke J, Tenthorey JL, Lee AY, Philip NH, Ayres JS, Brodsky IE, Gronert K, Vance RE. 2017. NAIP-NLRC4 Inflammasomes Coordinate Intestinal Epithelial Cell Expulsion with Eicosanoid and IL-18 Release via Activation of Caspase-1 and -8. *Immunity* **46**:649–659. doi:10.1016/j.immuni.2017.03.016

Ravichandran KS. 2011. Beginnings of a Good Apoptotic Meal: The Find-Me and Eat-Me Signaling Pathways. *Immunity* **35**:445–455. doi:10.1016/j.immuni.2011.09.004

Rong Fu Wang, Kushner SR. 1991. Construction of versatile low-copy-number vectors for cloning, sequencing and gene expression in Escherichia coli. *Gene* **100**:195–199. doi:10.1016/0378-1119(91)90366-J

Saha B, Bhattacharjee S, Sarkar A, Bhor R, Pai K, Bodhale N. 2021. Conundrums in leishmaniasis. *Cytokine* **145**. doi:10.1016/J.CYTO.2020.155304

Salcedo SP, Noursadeghi M, Cohen J, Holden DW. 2001. Intracellular replication of Salmonella typhimurium strains in specific subsets of splenic macrophages in vivo. *Cell Microbiol* **3**:587–597. doi:10.1046/J.1462-5822.2001.00137.X

Sellin ME, Müller AA, Felmy B, Dolowschiak T, Diard M, Tardivel A, Maslowski KM, Hardt WD. 2014. Epithelium-Intrinsic NAIP/NLRC4 Inflammasome Drives Infected Enterocyte Expulsion to Restrict Salmonella Replication in the Intestinal Mucosa. *Cell Host Microbe* **16**:237–248. doi:10.1016/J.CHOM.2014.07.001

Shornick LP, De Togni P, Mariathasan S, Goellner J, Strauss-Schoenberger J, Karr RW, Ferguson TA, Chaplin DD. 1996. Mice deficient in IL-1beta manifest impaired contact hypersensitivity to trinitrochlorobenzone. *J Exp Med* **183**:1427–1436. doi:10.1084/JEM.183.4.1427

Takeda K, Tsutsui H, Yoshimoto T, Adachi O, Yoshida N, Kishimoto T, Okamura H, Nakanishi K, Akira S. 1998. Defective NK cell activity and Th1 response in IL-18-deficient mice. *Immunity* **8**:383–390. doi:10.1016/S1074-7613(00)80543-9

Theisen E, Sauer JD. 2017. Listeria monocytogenes-induced cell death inhibits the generation of cell- mediated immunity. *Infect Immun* **85**. doi:10.1128/IAI.00733-16

Thurston TLM, Matthews SA, Jennings E, Alix E, Shao F, Shenoy AR, Birrell MA, Holden DW. 2016. Growth inhibition of cytosolic Salmonella by caspase-1 and caspase-11 precedes host cell death. *Nat Commun* **7**. doi:10.1038/NCOMMS13292

Tsuchiya K, Nakajima S, Hosojima S, Thi Nguyen D, Hattori T, Manh Le T, Hori O, Mahib MR, Yamaguchi Y, Miura M, Kinoshita T, Kushiyama H, Sakurai M, Shiroishi T, Suda T. 2019. Caspase-1 initiates apoptosis in the absence of gasdermin D. *Nat Commun* **10**:1–19. doi:10.1038/s41467-019-09753-2

Valenti M, Molina M, Cid VJ. 2022. Human Gasdermin D and MLKL disrupt mitochondria, endocytic traffic and TORC1 signaling in budding yeast. *bioRxiv* 2022.11.29.518328. doi:10.1101/2022.11.29.518328

Western blot membrane stripping for restaining protocol | Abcam. n.d. https://www.abcam.com/protocols/western-blot-membrane-stripping-for-restaining-protocol

Xia S, Zhang Z, Magupalli VG, Pablo JL, Dong Y, Vora SM, Wang L, Fu TM, Jacobson MP, Greka A, Lieberman J, Ruan J, Wu H. 2021. Gasdermin D pore structure reveals preferential release of mature interleukin-1. *Nature* **593**:607. doi:10.1038/S41586-021-03478-3

Yin XM, Wang K, Gross A, Zhao Y, Zinkel S, Klocke B, Roth KA, Korsmeyer SJ. 1999. Bid-deficient mice are resistant to Fas-induced hepatocellular apoptosis. *Nature 1999 400:6747* **400**:886–891. doi:10.1038/23730

Zhang L, Chen S, Ruan J, Wu J, Tong AB, Yin Q, Li Y, David L, Lu A, Wang WL, Marks C, Ouyang Q, Zhang X, Mao Y, Wu H. 2015. Cryo-EM structure of the activated NAIP2-NLRC4 inflammasome reveals nucleated polymerization. *Science* **350**:404. doi:10.1126/SCIENCE.AAC5789

Figures and Tables

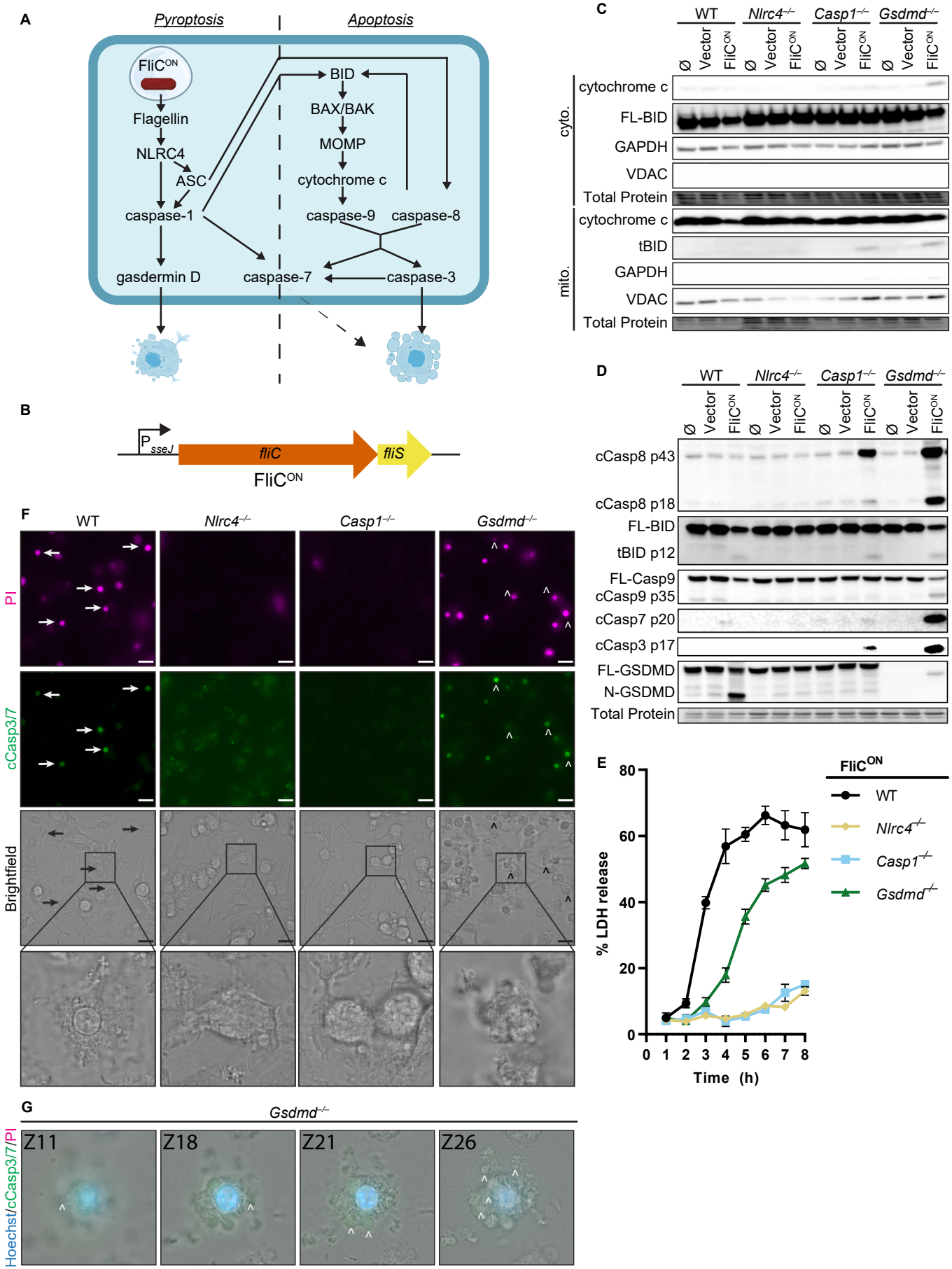
A
Pyroptosis
Apoptosis
FliC^ON
Flagellin
NLRC4
ASC
caspase-1
gasdermin D
BID
BAX/BAK
MOMP
cytochrome c
caspase-9
caspase-8
caspase-7
caspase-3
B
P sseJ
fliC
fliS
FliC^ON
C
WT
Nlrc4-/-
Casp1-/-
Gsdmd-/-
Ø
Vector
FliC^ON
cyto.
mito.
cytochrome c
FL-BID
GAPDH
VDAC
Total Protein
tBID
D
cCasp8 p43
cCasp8 p18
FL-BID
tBID p12
FL-Casp9
cCasp9 p35
cCasp7 p20
cCasp3 p17
FL-GSDMD
N-GSDMD
Total Protein
E
% LDH release
Time (h)
FliC^ON
WT
Nlrc4-/-
Casp1-/-
Gsdmd-/-
F
WT
Nlrc4-/-
Casp1-/-
Gsdmd-/-
PI
cCasp3/7
Brightfield
G
Gsdmd-/-
Hoechst/cCasp3/7/PI
Z11
Z18
Z21
Z26

Figure 1. FliC^{ON} *S.* Typhimurium activates apoptotic backup pathways in vitro.
A) Cell death pathways activated by FliC^{ON} *S.* Typhimurium.
B) Schematic of engineered FliC^{ON} construct.
C-F) BMMs were infected with indicated SPI2-induced *S.* Typhimurium strains.
C) Western blot analysis of cytosolic and mitochondrial fractions at 5 hpi. Representative image from three independent experiments.
D) Western blot analysis of whole cell lysates at 4 hpi. Representative image from three independent experiments.
E) LDH release at 1-8 hpi. Results representative of 3 independent experiments. Data are represented as mean ± SD of 3 technical replicates.
F-G) Immunofluorescence and brightfield. Cells were stained with PI, cleaved caspase-3/7, and Hoechst.
F) Representative image from two (brightfield, PI) or one (cleaved caspase-3/7) independent experiments at 4hpi. 60x magnification, scale bar 20µm. Arrows, pyroptotic cells. Carrots, apoptotic cells.
G) Z-stack slices from Movie S1. *Gsdmd*$^{-/-}$ BMMs infected with FliC^{ON} imaged at 6 hpi. Representative Z-stack from three (brightfield, PI) or one (cleaved caspase-3/7) independent experiments. 60x magnification, Z-slices 11, 18, 21, and 26 shown. Carrots; selected examples of apoptotic bodies.

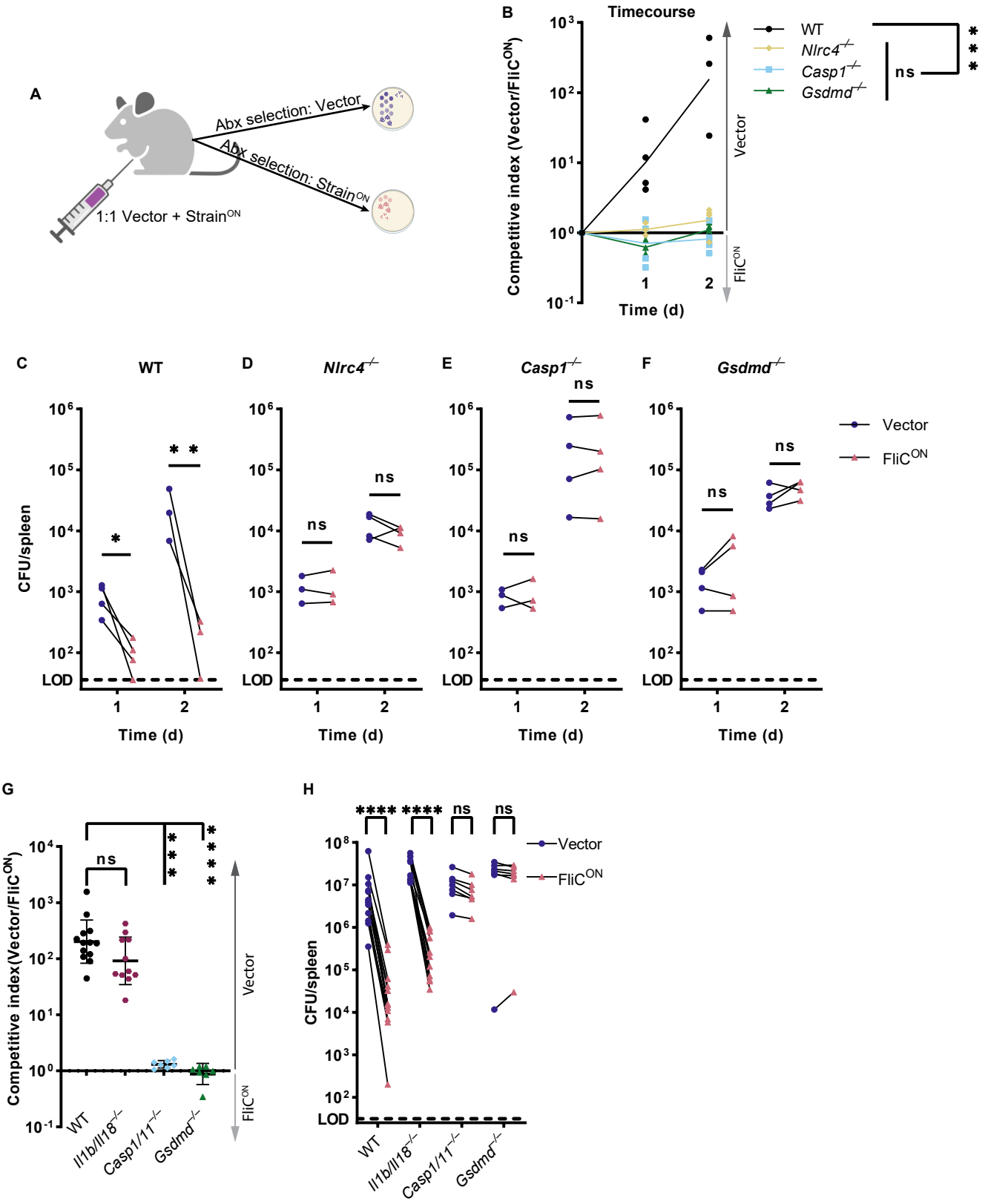
A
Abx selection: Vector
Abx selection: Strain^ON
1:1 Vector + Strain^ON
B
Timecourse
Competitive index (Vector/FliC^ON)
Time (d)
WT
Nlrc4-/-
Casp1-/-
Gsdmd-/-
ns
Vector
FliC^ON
C
WT
D
Nlrc4-/-
E
Casp1-/-
F
Gsdmd-/-
CFU/spleen
LOD
Time (d)
Vector
FliC^ON
G
Competitive index(Vector/FliC^ON)
WT
Il1b/Il18-/-
Casp1/11-/-
Gsdmd-/-
H
CFU/spleen
LOD
Vector
FliC^ON

Figure 2. Backup apoptosis does not clear FliC^{ON} *S.* Typhimurium in the spleen.
A) Schematic of competitive index infection model.
B-H) Mice were infected with a 1:1 ratio of FliC^{ON} and a vector control *S.* Typhimurium. Bacterial burdens in the spleen were determined at the indicated timepoints.
B) Timecourse of competitive index infection in indicated mice. Mice were infected with $5x10^2$ CFU of each strain. Ratio of vector to FliC^{ON} is graphed. Data representative of three (WT, *Gsdmd*$^{-/-}$) or two (*Nlrc4*$^{-/-}$, *Casp1*$^{-/-}$) independent experiments. Line connects mean, two-way ANOVA n.s. $p>0.05$; *** $p<0.001$.
C-F) Individual burdens of vector and FliC^{ON} from (B). Paired vector and FliC^{ON} data from each mouse are connected by a line. Two-way repeated measure ANOVA. n.s. $p>0.05$, *$p<0.05$, ** $p<0.01$
G) Mice were infected with $5x10^4$ CFU of each strain. Bacterial burdens in the spleen were determined at 48 hpi. Ratio of vector to FliC^{ON} is graphed. Combined two independent experiments, line representing mean ± SD, N=7-13 mice per genotype. Kruskal-Wallis n.s. $p>0.05$; *** $p<0.001$, ****$p<0.0001$.
H) Individual burdens from (G). Paired vector and FliC^{ON} data from each mouse are connected by a line. Two-way repeated measure ANOVA. n.s. $p>0.05$, ****$p<0.0001$

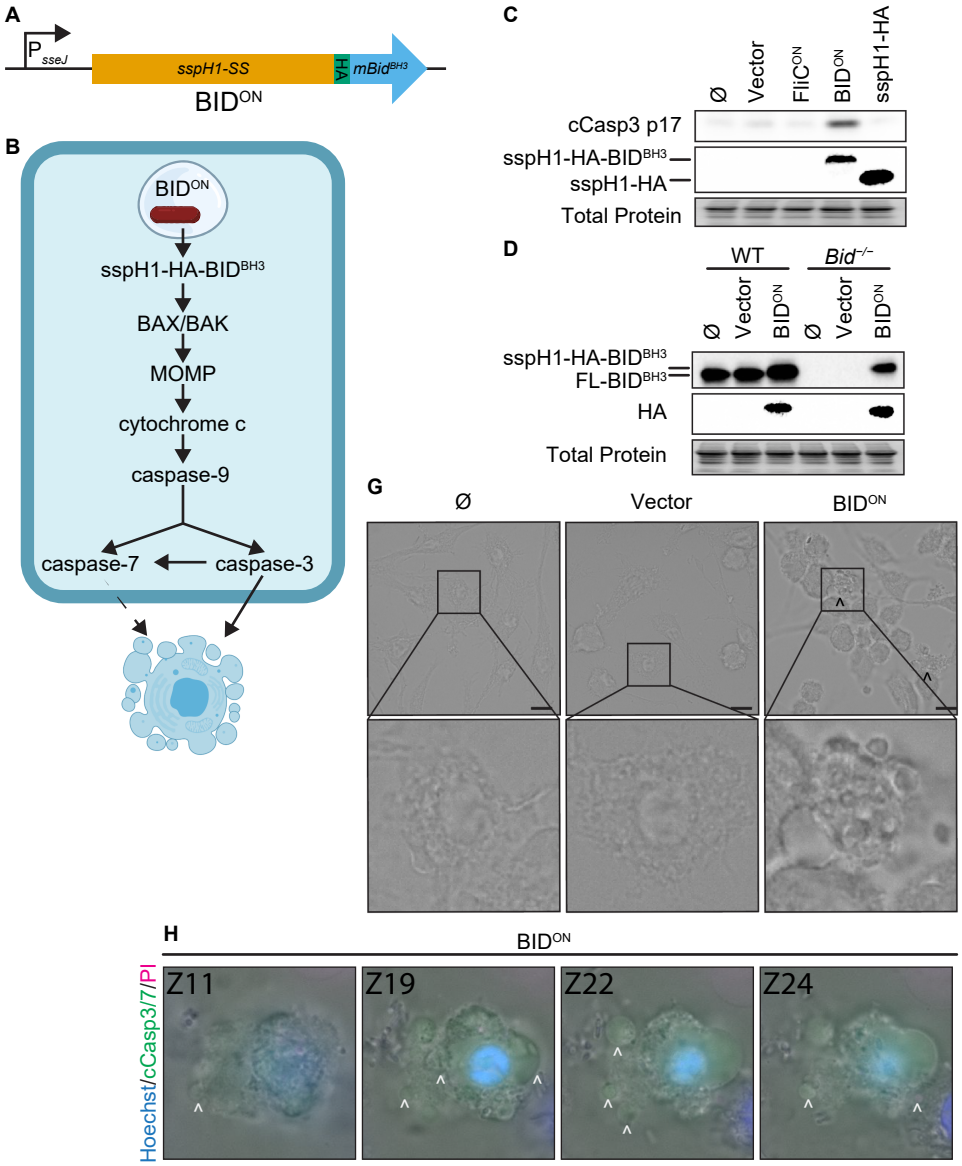
A
P sseJ
sspH1-SS
HA
mBid BH3
BIDON
B
BIDON
sspH1-HA-BIDBH3
BAX/BAK
MOMP
cytochrome c
caspase-9
caspase-7
caspase-3
C
Ø
Vector
FliCON
BIDON
sspH1-HA
cCasp3 p17
sspH1-HA-BIDBH3
sspH1-HA
Total Protein
D
WT
Bid-/-
Ø
Vector
BIDON
Ø
Vector
BIDON
sspH1-HA-BIDBH3
FL-BIDBH3
HA
Total Protein
E
WT
Ø
Vector
BIDON
cCasp8 p43
cCasp8 p18
sspH1-HA-BIDBH3
FL-BIDBH3
HA
FL-Casp9
cCasp9 p35
cCasp7 p20
cCasp3 p17
FL-GSDMD
N-GSDMD
Total Protein
F
WT
Ø
Vector
BIDON
cyto.
cytochrome c
GAPDH
VDAC
Total Protein
mito.
cytochrome c
GAPDH
VDAC
Total Protein
G
Ø
Vector
BIDON
H
BIDON
Hoechst/cCasp3/7/PI
Z11
Z19
Z22
Z24

Figure 3. Engineered BID^{ON} *S.* Typhimurium activates apoptosis in vitro.
A) Schematic of engineered BID^{ON} construct.
B) Pathway model showing how BID^{ON} leads to intrinsic apoptosis.
C-G) BMMs were infected with indicated SPI2-induced *S.* Typhimurium strains.
C-E) Western blot analysis of whole cell lysates at 6 hpi. Data representative of two (C) or three (D-E) independent experiments.
F) Western blot analysis of cytosolic and mitochondrial fractions at 4 hpi. Data representative from three independent experiments.
G) Brightfield at 6 hpi. Data representative of three independent experiments. 60x magnification, scale bar 20 µm, carrot, apoptotic blebs.
H) Z-stack slices from Movie S2. WT BMMs infected with BID^{ON} imaged at 6 hpi. Representative Z-stack from three (brightfield, PI) or one (cleaved caspase-3/7) independent experiments. 60x magnification, Z-slices 11, 19, 22, and 24 shown. Carrots; selected examples of apoptotic bodies.

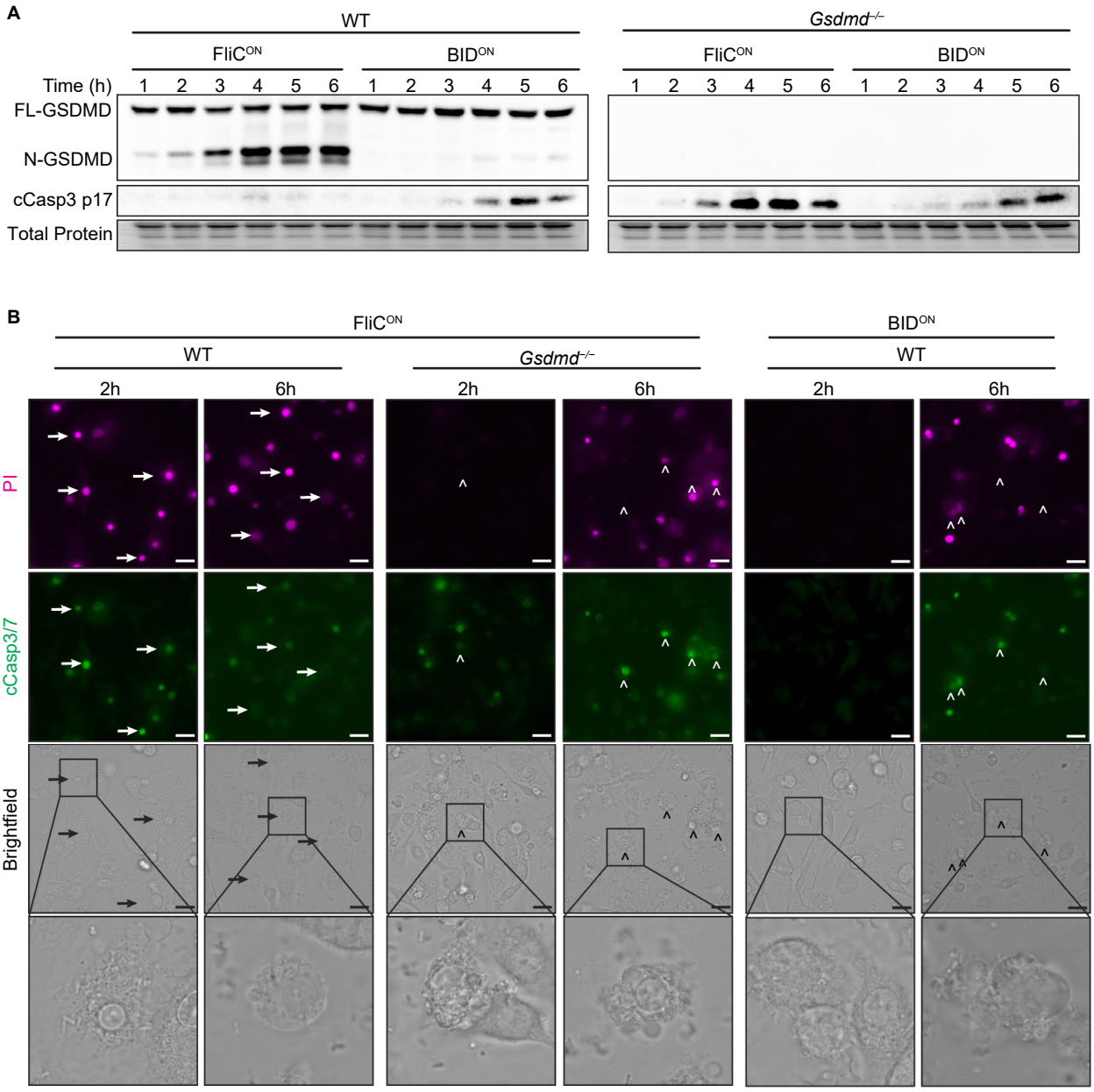
A
WT
Gsdmd-/-
FliCON
BIDON
FliCON
BIDON
Time (h)
1 2 3 4 5 6 1 2 3 4 5 6
1 2 3 4 5 6 1 2 3 4 5 6
FL-GSDMD
N-GSDMD
cCasp3 p17
Total Protein
B
FliCON
BIDON
WT
Gsdmd-/-
WT
2h
6h
2h
6h
2h
6h
PI
cCasp3/7
Brightfield

Figure 4. Apoptosis is induced slower than pyroptosis.
A-B) BMMs were infected with indicated SPI2-induced *S.* Typhimurium strains.
A) Western blot analysis of whole cell lysates. Representative of five independent experiments.
B) Immunofluorescence and brightfield. Cells were stained with PI, cleaved caspase-3/7, and Hoechst and imaged at indicated timepoints. Representative image from three (brightfield, PI) or one (cleaved caspase-3/7) independent experiments. Z-stack of the 6h timepoint are represented in Movies S1-2. Z-stack slice 19 ($FliC^{ON}$ in *Gsdmd*$^{-/-}$) and slice 20 (BID^{ON} in WT) shown here. 60x magnification, scale bar 20µm. Arrows, pyroptotic cells. Carrots, apoptotic cells.

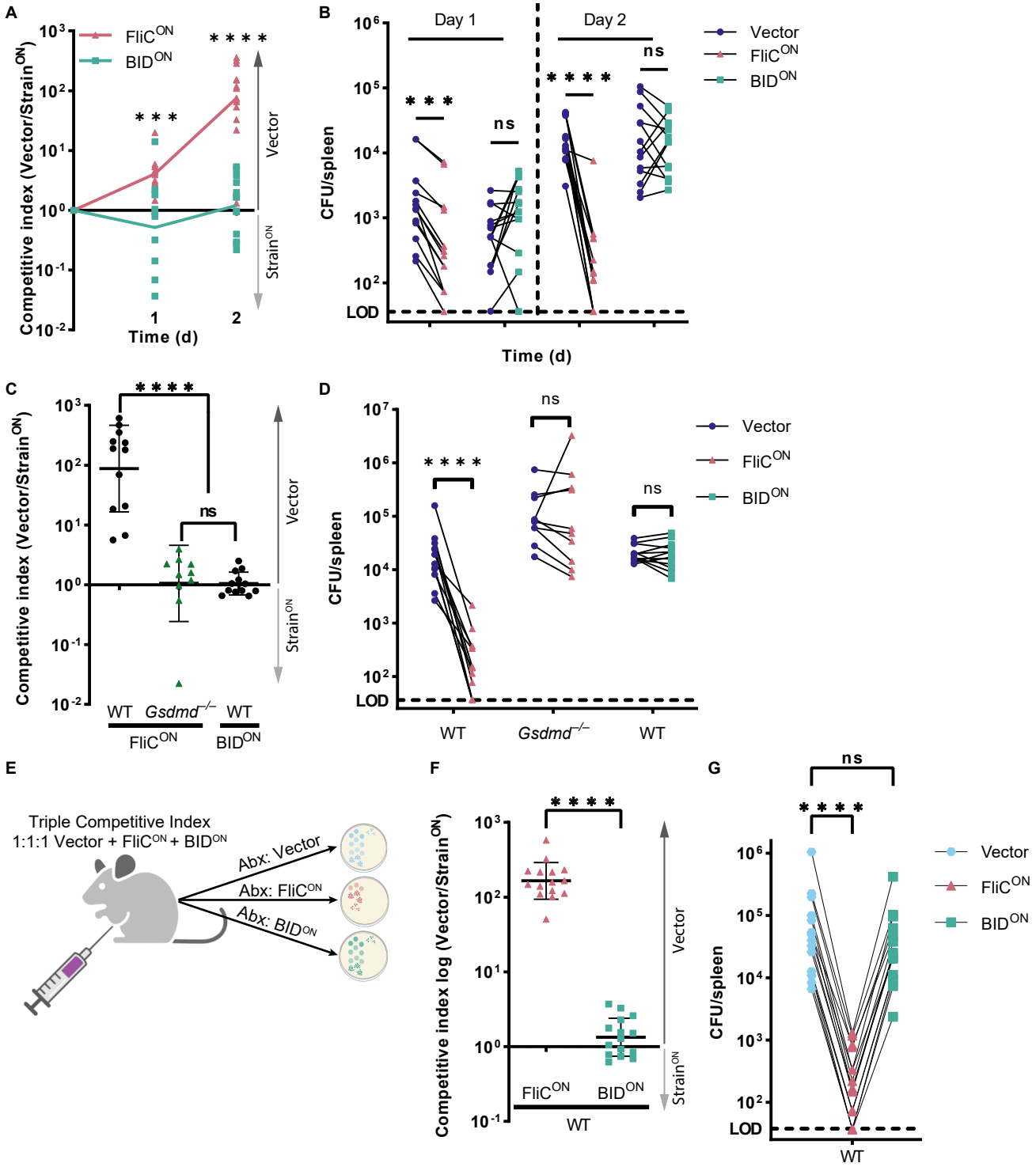
A
FliC^ON
BID^ON
Competitive index (Vector/Strain^ON)
Time (d)
Vector
Strain^ON
B
Day 1
Day 2
CFU/spleen
LOD
Time (d)
Vector
FliC^ON
BID^ON
C
Competitive index (Vector/Strain^ON)
WT
Gsdmd−/−
FliC^ON
BID^ON
D
CFU/spleen
LOD
WT
Gsdmd−/−
E
Triple Competitive Index
1:1:1 Vector + FliC^ON + BID^ON
Abx: Vector
Abx: FliC^ON
Abx: BID^ON
F
Competitive index log (Vector/Strain^ON)
FliC^ON
BID^ON
WT
G
CFU/spleen
LOD
WT

Figure 5. Intrinsic apoptosis does not clear engineered *S*. Typhimurium in the spleen.
A-D) Mice were infected with a 1:1 ratio of either FliC^{ON} or BID^{ON} and a vector control *S.* Typhimurium. Mice were infected with $5x10^2$ CFU of each strain. Bacterial burdens in the spleen were determined at the indicated timepoints.
A) Timecourse competitive index infection in WT mice. Ratio of vector to either FliC^{ON} or BID^{ON} is graphed. Data is combined from three independent experiments, line connects means, N=13-14 mice per condition. Two-way ANOVA *** $p<0.001$, ****$p<0.0001$.
B) Individual burdens of vector and FliC^{ON} or BID^{ON} from (A). Paired vector and FliC^{ON} or BID^{ON} data from each mouse are connected by a line. Two-way repeated measure ANOVA n.s. $p>0.05$; *** $p<0.001$, ****$p<0.0001$.
C) Competitive index infection of indicated mice infected with either FliC^{ON} or BID^{ON}. Ratio of vector to either FliC^{ON} or BID^{ON} is graphed. Bacterial burdens in the spleen were determined at 48 hpi. Data is combined from three independent experiments, line representing mean ± SD, N=10-12 mice per condition. One-way ANOVA n.s. $p>0.05$, ****$p<0.0001$
D) Individual burdens of vector and FliC^{ON} or BID^{ON} from (C). Paired vector and Strain^{ON} data from each mouse are connected by a line. Two-way repeated measure ANOVA n.s. $p>0.05$, ****$p<0.0001$
E) Schematic of triple competitive index model.
F-G) Mice were infected simultaneously with three strains, $5x10^2$ CFU each of vector (Cam), FliC^{ON} (Kan), and BID^{ON} (Amp) *S*. Typhimurium. Bacterial burdens in the spleen were determined at 48 hpi.
F) Triple competitive index infection of WT mice. Ratio of vector (Cam) to FliC^{ON} (Kan) or BID^{ON} (Amp) is graphed. Data is combined from three independent experiments, line representing mean ±SD, N=15. Unpaired two-tailed t-test ****$p<0.0001$.
G) Individual burdens of vector (Cam), FliC^{ON} (Kan), and BID^{ON} (Amp) from (F). Paired vector, FliC^{ON}, and BID^{ON} data from each mouse are connected by a line. Two-way repeated measure ANOVA n.s. $p>0.05$, ****$p<0.0001$.

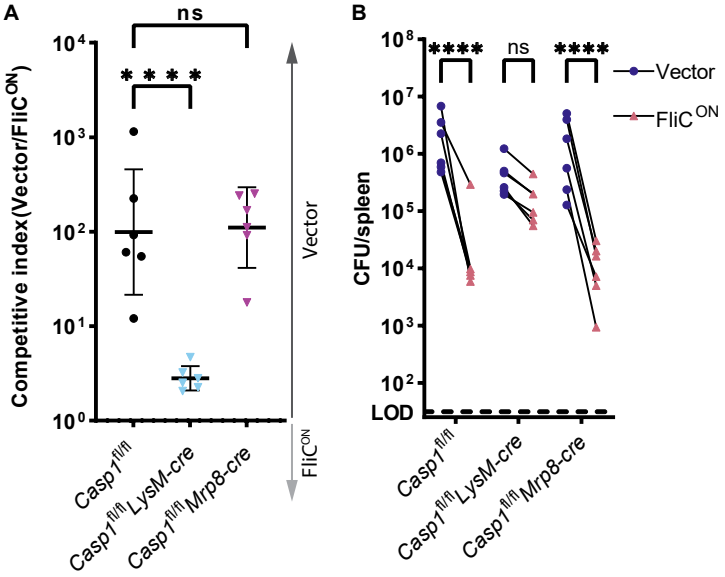
A
ns
****
Competitive index(Vector/FliC^ON)
10^4
10^3
10^2
10^1
10^0
Vector
FliC^ON
Casp1^fl/fl
Casp1^fl/fl LysM-cre
Casp1^fl/fl Mrp8-cre
B
****
ns
****
Vector
FliC^ON
CFU/spleen
10^8
10^7
10^6
10^5
10^4
10^3
10^2
LOD
Casp1^fl/fl
Casp1^fl/fl LysM-cre
Casp1^fl/fl Mrp8-cre

Figure 6. Pyroptosis clears FliC^{ON} from myeloid compartment in vivo.
A) Mice were infected with $5x10^4$ CFU of each strain. Bacterial burdens in the spleen were determined at 48 hpi. Ratio of vector to FliC^{ON} is graphed. Combined two independent experiments, line representing mean ± SD, N=6 mice per genotype. One-way ANOVA n.s. $p>0.05$; ****$p<0.0001$.
B) Individual burdens from (A). Paired vector and FliC^{ON} data from each mouse are connected by a line. Two-way repeated measure ANOVA. n.s. $p>0.05$, ****$p<0.0001$

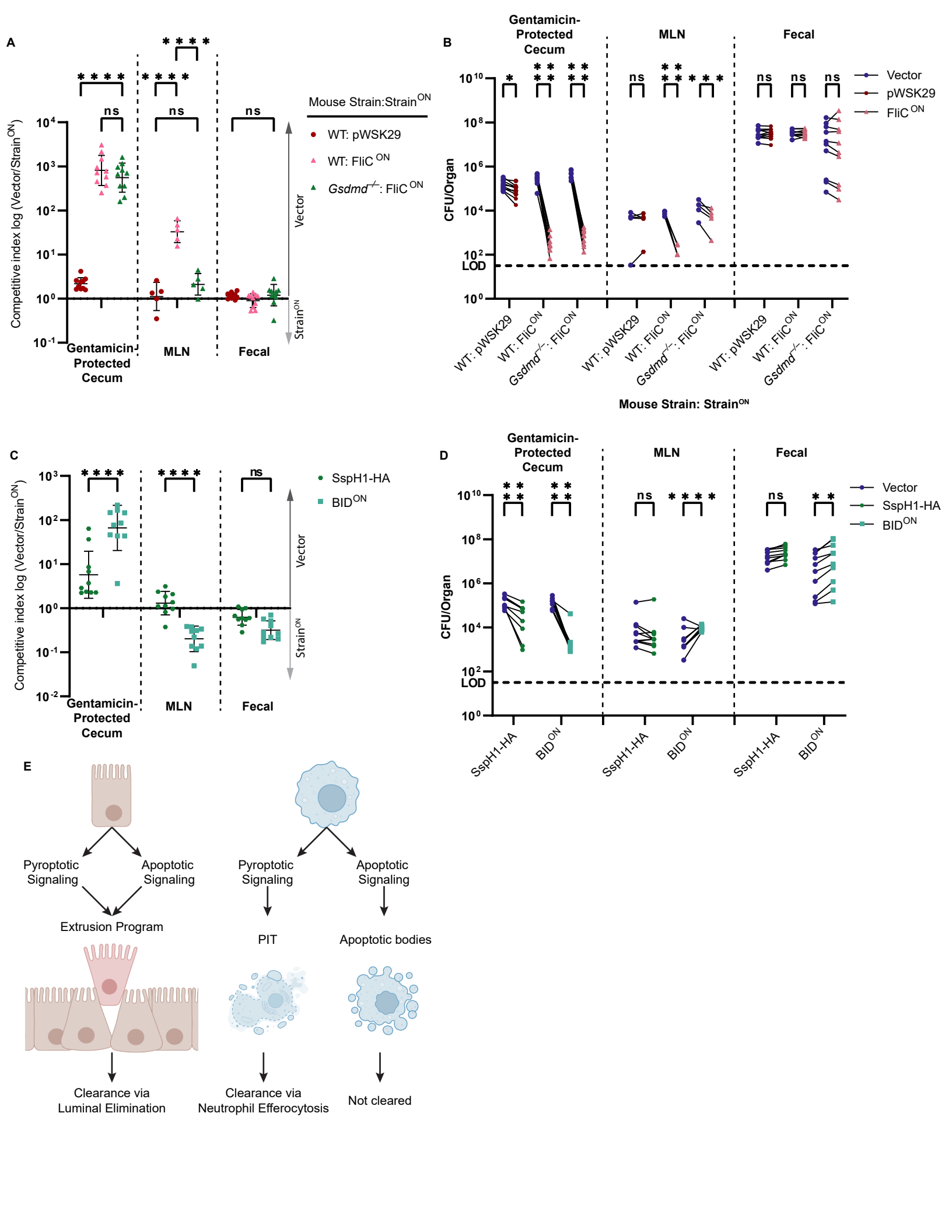
A
Competitive index log (Vector/Strain^{ON})
Gentamicin-Protected Cecum
MLN
Fecal
ns
Mouse Strain:Strain^{ON}
WT: pWSK29
WT: FliC^{ON}
Gsdmd$^{-/-}$: FliC^{ON}
Vector
Strain^{ON}
B
CFU/Organ
LOD
Vector
pWSK29
FliC^{ON}
Mouse Strain: Strain^{ON}
C
SspH1-HA
BID^{ON}
D
E
Pyroptotic Signaling
Apoptotic Signaling
Extrusion Program
PIT
Apoptotic bodies
Clearance via Luminal Elimination
Clearance via Neutrophil Efferocytosis
Not cleared

Figure 7. Apoptotic pathways lead to clearance in the cecum.
A-D) Mice were orally treated with 20mg streptomycin, and 24h later orally infected with $1x10^7$ CFUs total bacteria comprised of a 1:1 ratio of the indicated ampicillin resistant strain and kanamycin resistant vector (pWSK129) control *S.* Typhimurium, all on a *flgB* mutant background. Bacterial burdens in the cecum, mesenteric lymph nodes (MLN), and fecal sample were determined at 48 hpi.
A) Competitive index is graphed as a ratio of vector to either pWSK29 or $FliC^{ON}$. Data is combined from two (cecum, fecal) or one (MLN) independent experiments (MLN was not harvested in the first experiment, where we harvested the spleen, which had negligible burdens; one additional representative experiment is shown in Figure S6A-B), line representing mean ± SD, N=10 (cecum, fecal) or 5 (MLN) mice per condition. Two-way repeated measure ANOVA n.s. $p>0.05$, ****$p<0.0001$.
B) Individual burdens of vector and pWSK29 or $FliC^{ON}$ from (A). Paired vector and $Strain^{ON}$ data from each mouse are connected by a line. Two-way repeated measure ANOVA n.s. $p>0.05$, *$p<0.05$, ***$p<0.001$, ****$p<0.0001$.
C) Competitive index infection of WT mice infected with either SspH1-HA or BID^{ON}. Ratio of vector to either SspH1-HA or BID^{ON} is graphed. Data is combined from two independent experiments, line representing mean ± SD, N=10 mice per condition. Two-way repeated measure ANOVA n.s. $p>0.05$, ****$p<0.0001$.
D) Individual burdens of vector and SspH1-HA or BID^{ON} from (C). Paired vector and $Strain^{ON}$ data from each mouse are connected by a line. Two-way repeated measure ANOVA n.s. $p>0.05$, **$p<0.01$, ****$p<0.0001$.
E) Schematic demonstrating the ability of pyroptotic or apoptotic signaling to lead to clearance of engineered *S.* Typhimurium in either IECs or macrophages.